AD-A069 624 PENNSYLVANIA STATE UNIV UNIVERSITY PARK APPLIED RESE--ETC F/G 20/13
AN INVESTIGATION OF A TWO-PHASE, MOVING BOUNDARY SYSTEM, WITH C--ETC(U)
JAN 79 M W NANSTEEL N00024-79-C-6043
UNCLASSIFIED ARL/PSU/TM-79-32 NL

1 OF 2
AD A069624

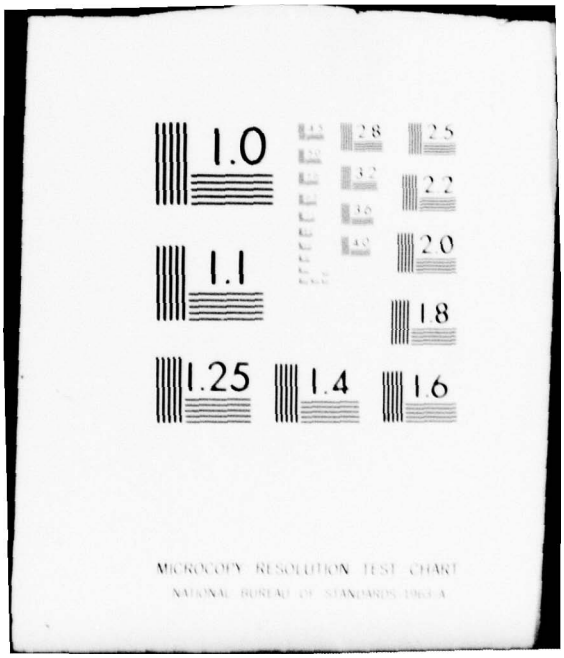
1.0
1.1
1.25
1.4
1.6
2.8
2.5
2.2
2.0
1.8
MICROCOPY RESOLUTION TEST CHART
NATIONAL BUREAU OF STANDARDS 1963-A

AN INVESTIGATION OF A TWO-PHASE, MOVING BOUNDARY SYSTEM, WITH CONVECTION AT THE SOLID-LIQUID INTERFACE

Mark Wayne Nansteel

Technical Memorandum
File No. TM 79-32
January 23, 1979
Contract No. N00024-79-C-6043

Copy No. 7

The Pennsylvania State University
Institute for Science and Engineering
APPLIED RESEARCH LABORATORY
Post Office Box 30
State College, PA 16801

NAVY DEPARTMENT

NAVAL SEA SYSTEMS COMMAND

UNCLASSIFIED

SECURITY CLASSIFICATION OF THIS PAGE (When Data Entered)

REPORT DOCUMENTATION PAGE

READ INSTRUCTIONS BEFORE COMPLETING FORM

1. REPORT NUMBER: TM 79-32

2. GOVT ACCESSION NO.:

3. RECIPIENT'S CATALOG NUMBER:

4. TITLE (and Subtitle): (6) AN INVESTIGATION OF A TWO-PHASE, MOVING BOUNDARY SYSTEM, WITH CONVECTION AT THE SOLID-LIQUID INTERFACE

5. TYPE OF REPORT & PERIOD COVERED: MS Thesis, May 1979

6. PERFORMING ORG. REPORT NUMBER: TM 79-32

7. AUTHOR(s): (10) Mark Wayne Nansteel

8. CONTRACT OR GRANT NUMBER(s): (15) N00024-79-C-6043

9. PERFORMING ORGANIZATION NAME AND ADDRESS:
The Pennsylvania State University
Applied Research Laboratory
P. O. Box 30, State College, PA 16801

10. PROGRAM ELEMENT, PROJECT, TASK AREA & WORK UNIT NUMBERS:

11. CONTROLLING OFFICE NAME AND ADDRESS:
Naval Sea Systems Command
Department of the Navy
Washington, DC 20362

12. REPORT DATE: (11) 23 Jan 79 — January 23, 1979

13. NUMBER OF PAGES: 143 pages & figures

14. MONITORING AGENCY NAME & ADDRESS (if different from Controlling Office):

15. SECURITY CLASS. (of this report): Unclassified, Unlimited

15a. DECLASSIFICATION/DOWNGRADING SCHEDULE:

16. DISTRIBUTION STATEMENT (of this Report)

Approved for public release, distribution unlimited,
per NSSC (Naval Sea Systems Command), 3/23/79

(12) 145 p.

17. DISTRIBUTION STATEMENT (of the abstract entered in Block 20, if different from Report)

(14) ARL/PSU/TM-79-32

18. SUPPLEMENTARY NOTES

(9) Technical memo.

19. KEY WORDS (Continue on reverse side if necessary and identify by block number)

two-phase
fusion
convection
boundary layer

20. ABSTRACT (Continue on reverse side if necessary and identify by block number)

An analytical and experimental study has been carried out in order to investigate the behavior of a two-phase, solid-liquid system in which the solid phase is subjected to varying heat flux and temperature at its boundaries.

The specific geometry chosen for the study was that of a thin solid layer formation on a planar surface which is maintained below the fusion temperature of the liquid. The determination of the phase boundary position was accomplished primarily by a variable nodal system finite difference technique. In addition, an integral solution similar to those frequently used in the

DD FORM 1 JAN 73 1473 EDITION OF 1 NOV 65 IS OBSOLETE

391 007

UNCLASSIFIED

SECURITY CLASSIFICATION OF THIS PAGE (When Data Entered)

20. ABSTRACT (Continued)

calculation of two-dimensional boundary layer flows in fluid dynamics is formulated and compared with the results of the finite difference technique. It is concluded that the integral solution is in many instances as effective a solution technique as the finite difference method.

An experimental study was carried out with ice and water in turbulent channel flow in order to test the validity of the mathematical model. The results of the experiment indicate that the model is capable of predicting the position of the phase interface to within limits of accuracy which are acceptable for most engineering applications. It is found that the model's inability to account for temperature dependent solid phase properties may have an adverse effect on its performance for substances whose transport properties are highly dependent upon temperature.

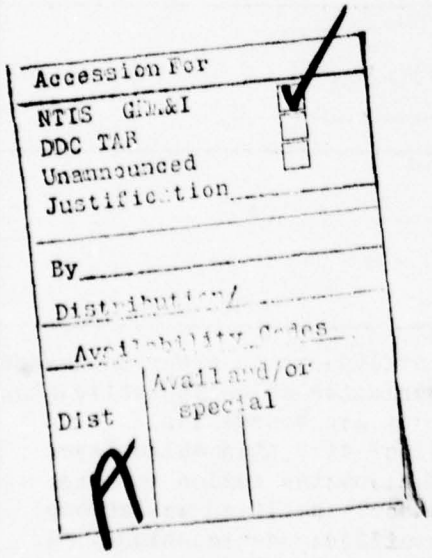

ABSTRACT

An analytical and experimental study has been carried out in order to investigate the behavior of a two-phase, solid-liquid system in which the solid phase is subjected to varying heat flux and temperature at its boundaries.

The specific geometry chosen for the study was that of a thin solid layer formation on a planar surface which is maintained below the fusion temperature of the liquid. The determination of the phase boundary position was accomplished primarily by a variable nodal system finite difference technique. In addition, an integral solution similar to those frequently used in the calculation of two-dimensional boundary layer flows in fluid dynamics is formulated and compared with the results of the finite difference technique. It is concluded that the integral solution is in many instances as effective a solution technique as the finite difference method.

An experimental study was carried out with ice and water in turbulent channel flow in order to test the validity of the mathematical model. The results of the experiment indicate that the model is capable of predicting the position of the phase interface to within limits of accuracy which are acceptable for most engineering applications. It is found that the model's inability to account for temperature dependent solid phase properties may have an adverse effect on its performance for substances whose transport properties are highly dependent upon temperature.

TABLE OF CONTENTS

TABLE OF CONTENTS (continued)

TABLE OF CONTENTS (continued)

LIST OF TABLES

LIST OF FIGURES

LIST OF FIGURES (continued)

LIST OF FIGURES (continued)

LIST OF SYMBOLS

Symbol	Description
A	arbitrary constant in Equation (28)
A_j	rational function coefficient
a_m	least squares polynomial coefficient
B	arbitrary constant in Equation (28)
B_k	rational function coefficient
b	constant defined by Equation (67)
C_1, C_2	coefficients in Equation (31)
c	heat capacity
D_1, D_2, D_3	coefficients in approximate solid layer temperature profile
D_h	hydraulic diameter of flow channel
$(DEV)_{max}$	maximum percentage deviation
$(DEV)_{rms}$	root mean square deviation
d	diameter of thermocouple probe
h	ice-water interface film coefficient
$\overline{h}$	average film coefficient over thermocouple probe shaft
h'	increased ice-water interface film coefficient
h_t	film coefficient at thermocouple probe tip
Δh	incremental increase in interface film coefficient
I	number of measurements used in rational function curve fit
J	degree of the numerator in rational function approximation
K	degree of the denominator in rational function approximation

LIST OF SYMBOLS (continued)

Symbol	Description
k	solid layer thermal conductivity
ℓ	latent heat of fusion
M	degree of least squares polynomial
N	total number of temperature nodes
Nu	Nusselt number based upon D_h
Nud	Nusselt number based upon d
Pr	Prandtl number
Q	volumetric flow rate
q'_c	increased ice-water interface heat flux
q''_c	ice-water interface heat flux
q*	dimensionless heat flux parameter
q^*_i	the value of q* for $t^* < 0$
Re	Reynolds number based upon D_h
Red	Reynolds number based upon d
S	solid layer thickness
S'	thickness of disturbed solid layer
S*	dimensionless solid layer thickness
S_o	solid layer thickness at $t^* = 0$
St	Stefan number
St_i	Stefan number for $t^* < 0$
T	temperature
T_b	bulk water temperature
T_F	fluid temperature in boundary layer
T_m	equilibrium melting temperature

LIST OF SYMBOLS (continued)

Symbol	Description
T_o	temperature in the solid layer at $t^* = 0$
T_w	wall temperature
T_{wi}	measured value of cooling plate surface temperature
T_∞	freestream temperature
t	time
t^*	dimensionless time
t_i	time corresponding to measurement of T_{wi}
Δt^*	time step in finite difference solution
V	flow velocity
Y	dimensionless position coordinate used in thermocouple probe analysis
y	position coordinate (solid layer)
y^*	dimensionless solid layer position coordinate
y^*_n	dimensionless position of the nth temperature node
Δy^*	instantaneous spacing between temperature nodes
Z	position coordinate used in thermocouple probe analysis

Greek Letters

α	thermal diffusivity
β	parameter defined by Equation (26)
δ	boundary layer thickness in thermocouple probe analysis
δ_t	thermal boundary layer thickness
δ_h	hydraulic boundary layer thickness
η	variable of integration
θ	dimensionless solid layer temperature

LIST OF SYMBOLS (continued)

Symbol	Description
θ_o	dimensionless solid layer temperature at $t^* = 0$
θ_n^r	θ at the nth node and rth time step in the finite difference solution
κ	exponent in turbulent temperature profile expression
Δ	dimensionless temperature in thermocouple probe analysis
Δ_F	dimensionless boundary layer fluid temperature
λ	effective thermocouple probe thermal conductivity
ν	kinematic viscosity
π	3.14159
ρ	mass density

ACKNOWLEDGEMENTS

The author extends his sincerest appreciation to Professor Carl H. Wolgemuth for his invaluable advice, criticism, and encouragement throughout this research.

The author is also appreciative of the support obtained from the Applied Research Laboratory of The Pennsylvania State University under contract with the Naval Sea Systems Command.

CHAPTER I

INTRODUCTION

A. Discussion of the Problem and Motivation for the Work

The study presented here was carried out in order to gain a better understanding of the phenomena occurring in a two-phase, solid-liquid system subjected to varied temperature and heat flux conditions at the system boundaries. In this case, the primary objective is the determination of the phase interface position as a function of time for a given set of boundary and initial conditions.

There are many industrial applications in which some knowledge of the behavior of such a two-phase system may be a primary factor in the design or operation of a given apparatus. Examples of such applications include thermal energy storage, food processing, metal casting, water desalinization, and the design and operation of cryogenic and liquid metal heat exchangers. The solidification problem becomes especially important in the consideration of nuclear reactor safety where molten core debris may solidify and block coolant flow passages during the postaccident heat removal process [see Cheung and Baker (1)].

There are several factors which are common to most solidification and melting phenomena of practical significance. First, there is a single, continuous phase boundary separating the solid and liquid phases in each case. The shape of the interface (planar, cylindrical, etc.) in general depends upon the specific configuration of the apparatus. (There

are some situations in which the solid phase may be dispersed throughout the liquid phase; however, this situation arises only when the liquid is sufficiently supercooled and will not be considered here.) Also, the boundary conditions on the solid phase are such that there is one fixed boundary and one free or moving boundary where the moving boundary is in direct contact with the liquid phase which may or may not be flowing in forced convection. These conditions are characteristic of the class of phase change phenomena often referred to as "moving boundary" or "Stefan-type" problems and describe the fundamental physical configuration to be studied here.

B. Previous Work in Phase Change Heat Transfer

The basic problem of heat transfer in a substance undergoing phase change has avoided general solution for a long time. The analytical difficulties which are encountered can be mainly attributed to the nonlinear character of the interface boundary condition associated with the governing energy equation. Put another way, the spatial domain on which the solution for the temperature field is sought changes continuously with time. This means that the extent of each phase as well as the temperature distribution in the phase are unknown initially and both must be determined simultaneously.

The techniques of solution which exist at this time are basically of three general types:

Analytical (Closed Form) Solutions in which a particular solution is formulated for a set of simplified boundary conditions (often rather restrictive and unrealistic from a practical point of view).

Approximate Solutions in which simplifying assumptions are made, usually in order to reduce the number of independent variables describing the system.

Full Finite Difference Techniques in which the energy conservation equation is solved in its most general form.

A brief description of each method is given below.

1. Analytical Solutions

Analytical solutions to the two-phase conduction problem are available for only a limited number of cases corresponding to very simple boundary conditions and are usually of limited practical interest. The classical example of a closed form solution is that given by Stefan (2). Stefan considered a semi-infinite region filled with the isothermal (at the fusion temperature) liquid phase, bounded by a plane wall (fixed boundary). At zero time, the wall surface temperature is stepped down to some temperature below the fusion temperature and held constant thereafter, thus initiating solid layer formation and growth. It is assumed that heat transfer in both phases is via conduction only. The solution for the temperature distribution in the solid is obtained through the introduction of a similarity variable and the phase boundary position is obtained as a simple, algebraic function of time.

A somewhat less restrictive result was obtained by Portnov (3) for the instance in which the liquid phase is not initially isothermal and the wall temperature is a function of time. The solution for the semi-infinite domain is obtained through Laplace transform methods and ultimately is found in terms of an infinite series. The utility of this

solution, however, is limited, according to Stephan (4), due to the difficulties encountered in the evaluation of the coefficients in the series.

It is apparent from just these two examples of closed form solutions that they are of limited applicability and that other methods must be developed in order to deal with problems of practical importance.

2. Approximate Techniques

The most popular approximate techniques for solving moving boundary problems are the integral methods in which the temperature profile in each phase is approximated by some convenient functional relationship such as a polynomial in powers of the spatial coordinate. The energy equation is then integrated with respect to the space variable between the moving and fixed boundaries using the approximate profile. This procedure results in an ordinary differential equation (in the one-dimensional case) for the phase boundary position as a function of time. The procedure described here parallels the integral techniques used in the analysis of two-dimensional boundary layer flows in fluid dynamics.

Integral-type analyses have been applied to moving boundary systems by Goodman (5), Libby and Chen (6), Savino and Siegel (7), and Stephan (4). The rather extensive experimental investigation carried out by Siegel and Savino yielded results which were in good agreement with their integral formulation. In general, the integral techniques represent a much simplified and more general method of solution in comparison to the closed form, analytic solutions while retaining a high degree of accuracy.

Other approximate methods which have been employed with success in phase change problems are the variational techniques originally

developed by Biot (8). A variational approach was applied to the case of constant wall temperature solidification by Lapadula and Mueller (9). This work resulted in solutions for the phase boundary position for very small and very large time, comparable in accuracy to the integral method used by Libby and Chen. More general variational techniques (based on the Lagrangian formalism) were employed by Bilenas and Jiji (10) in a solution of the free boundary solidification problem with internal liquid flow. The results of this approximate analysis, however, deviated as much as $\pm$15% from the supposedly exact full finite difference solutions.

On the whole, variational methods are not as popular as integral methods, and integral methods therefore are responsible for the bulk of the approximate solutions.

3. Full Finite Difference Techniques

The third major category of solution methods are the numerical finite difference techniques. The principal advantage of numerical solution, of course, lies in the capability of these methods to handle irregular geometries, time varying boundary conditions, etc.. But even finite difference methods are adversely affected by the moving boundary characteristic of all phase change phenomena. In fixed nodal arrangements, the solid-liquid interface must move toward, reach, and pass-by each stationary temperature node so that when the interface is located between two nodes, its exact position is unknown and therefore it must be located approximately by interpolation. A continuous account of fusion front travel then becomes somewhat of a problem. The difference equations and interpolation formulae can become very complex, especially

when solution in two space variables is considered. For example, see Springer and Olson (11).

A unique nodal scheme for one-dimensional problems which eliminates the need for interpolation and yields a continuous, accurate account of the fusion front motion was suggested by Murray and Landis (12). In this nodal arrangement, the nodal mesh changes continuously with fusion front travel so that the interface position is always coincident with a temperature node; thus, there is no need for interpolation and the difference formulae are simplified considerably.

C. The Scope and Objectives of the Present Work

The purpose of the present study is twofold. First, it is desired to formulate a mathematical model which may be used to predict the phase boundary position as a function of time in a two-phase, solid-liquid system similar to those described above. The model accounts for one-dimensional heat flow in the solid phase and completely arbitrary forms of initial and boundary conditions. The primary method of analysis is based upon a variable nodal system finite difference method in the solid phase similar to that used by Murray and Landis (12). In the formulation of the model, it is assumed that the mechanism of heat transfer to the moving phase change interface is by convection from the flowing liquid because this condition represents a more practically important case than that of pure conduction heat transfer in the liquid. In addition, an integral solution is formulated under the same assumptions as those made for the full finite difference model. The two solution methods are compared both qualitatively and quantitatively in order to determine some of the advantages and disadvantages of integral representation as opposed to full numerical solution.

Secondly, an experimental investigation is carried out in order to test the analytical procedures discussed above for boundary and initial conditions representative of those which might be encountered in actual phase change phenomena. The experiment incorporates water in turbulent channel flow over a planar ice-water interface. The transient growth behavior of the solid phase is studied and compared directly with the analytically generated solutions for the phase boundary position. On the basis of this comparison, the validity and applicability of the solution techniques is evaluated.

CHAPTER II

ANALYSIS

A. Statement of the Problem

Figure 1 shows a two-phase system of solid and liquid in which the solid layer is bounded on one side by a planar, rigid wall and on the other side by the flowing liquid phase. The wall is assumed to be either a plane wall or one in which the local radius of curvature is large with respect to the local solid layer thickness, S. At the solid-liquid interface, $y = S$, the solid phase surface is subject to the convective heat flux from the warmer liquid which is a function of the local convective conductance, h, and the freestream temperature, T_∞. At $y = 0$, the layer is in direct contact with the solid wall which is assumed always to be at some temperature lower than the fusion temperature of the liquid; hence, some solid is always present. The assumption of direct contact between the solid layer and wall implies the absence of any contact resistance and, therefore, the temperature of the solid at $y = 0$ is equal to the wall temperature. It is important to note that, in this analysis, no assumptions will be made regarding the form of the time variations of wall temperature and interfacial heat flux. On the other hand, both T_w and q''_c must be known as functions of time before the problem solution can begin. Specification of the heat flux at the interface implies that the fluid dynamical problem for the region $y > S$ is independent of the solid layer thickness. This can

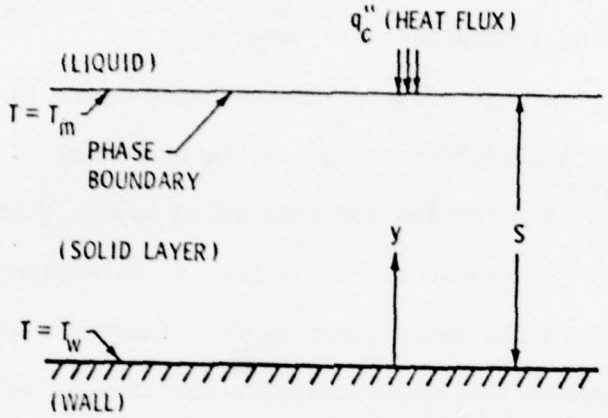

Figure 1. Sketch Illustrating the Basic Arrangement of Rigid Wall, Solid Layer, and Liquid Freestream

usually be justified as a reasonable assumption in external flow situations when S is small, but for internal flows when the layer thickness becomes appreciable in comparison with the flow radius, this assumption can no longer be made. A more complete discussion of the assumptions made in the analysis are given below.

B. Basic Assumptions in Model Formulation

The following assumptions are made:

1. Conduction heat transfer in the solid layer is primarily one-dimensional and in a direction normal to the solid wall. The validity of this assumption is justified for thin solid layers through a comparison of the steady-state heat fluxes in the y direction and in the direction parallel to the solid layer surface (near the wall). This comparison was accomplished experimentally and it was found that the flux in the y direction is always at least two orders of magnitude greater than in any other direction.

2. The wall temperature, T_w, and the convective heat flux at the interface, q''_c, are not dependent upon the solid layer thickness.

3. The material under consideration is a pure substance. The complexities which arise due to phase change temperature ranges and solid state phase transformations in multicomponent systems are not considered here. With respect to alloy systems, for example, Friedman (13) has approached the phase change problem successfully with a finite element technique; however, the present analysis will apply only to pure substances, homogeneous in the solid phase.

4. All solid properties are temperature independent. This assumption should not severely affect the accuracy of the results in

problems where temperature differences are not extreme, or where properties are not strongly dependent on temperature.

5. Thermodynamic equilibrium prevails at the solid-liquid interface.

C. Governing Equations

For the assumptions stated above, conservation of energy in the solid layer and at the phase change interface yield the following system:

$$\alpha \frac{\partial^2 T}{\partial y^2} = \frac{\partial T}{\partial t} \quad , \qquad 0 < y < S \tag{1a}$$

$$\left.\begin{aligned} T &= T_o(y) \quad , \qquad (1b) \\ S &= S_o \quad , \qquad (1c) \end{aligned}\right\} \quad t = 0$$

$$T = T_w \quad , \qquad y = 0 \tag{1d}$$

and

$$\left.\begin{aligned} T &= T_m \quad , \qquad (1e) \\ k \frac{\partial T}{\partial y} - q_c'' &= \rho \ell \frac{dS}{dt} \qquad (1f) \end{aligned}\right\} \quad y = S$$

The analytical difficulties which arise in the solution of Equations (1) are mainly due to the condition (1f) at the phase boundary. Consider the temperature field in the layer,

$$T = T[y,t] \quad . \tag{2}$$

At the interface, $y = S$,

$$dT = \left(\frac{\partial T}{\partial y}\right) dy + \left(\frac{\partial T}{\partial t}\right) dt = 0 \quad . \tag{3}$$

Rearranging and substituting into condition (1f) yields:

$$k \frac{\partial T}{\partial y} - q''_c = -\rho \ell \left[\frac{\partial T}{\partial t} / \frac{\partial T}{\partial y}\right] \quad . \tag{4}$$

The interface boundary condition is therefore seen to be nonlinear.

The system (1) is nondimensionalized by defining the following dimensionless groups:

$$y^* = \frac{y}{S_o} \quad , \quad t^* = \frac{t\alpha}{S_o^2} \quad , \quad \theta = \frac{T-T_w}{T_m-T_w} \quad , \quad S^* = \frac{S}{S_o} \quad ,$$

where $S_o > 0$ denotes the solid layer thickness at zero time, $t = t^* = 0$.

Substituting into Equations (1) results in,

$$\frac{\partial^2 \theta}{\partial y^{*2}} = \frac{1}{St} \frac{dSt}{dt^*} [\theta - 1] + \frac{\partial \theta}{\partial t^*} \quad , \qquad 0 < y^* < S^* \tag{5a}$$

$$\left.\begin{aligned} \theta &= \theta_o(y^*) \quad , \\ S^* &= 1 \quad , \end{aligned}\right\} \qquad t^* = 0 \tag{5b, 5c}$$

$$\theta = 0 \quad , \qquad y^* = 0 \tag{5d}$$

$$\theta = 1 \qquad \left.\right\} \qquad y^* = S^* \tag{5e}$$

and

$$St \frac{\partial \theta}{\partial y^*} - q^* = \frac{dS^*}{dt^*} \quad , \qquad \left.\right\} \tag{5f}$$

where the parameter, St (Stefan number), is defined by:

$$St = \frac{c(T_m - T_w)}{\ell} \quad , \tag{6}$$

and the dimensionless heat flux parameter by:

$$q^* = \frac{q''_c S_o}{\ell \rho \alpha} \quad . \tag{7}$$

Equations (5) completely define the problem studied here. It has been shown that the condition (5f) renders the system nonlinear and thereby makes closed form analytical solutions very difficult to obtain for all but the most elementary forms of boundary and initial conditions. The following sections briefly describe three methods of solution, of varying degrees of generality, which under the appropriate circumstances are found to yield accurate results for the phase change interface position, $S^*(t^*)$.

The first solution (asymptotic) is a result of neglecting the specific heat capacity of the solid phase in comparison to the latent heat of fusion. This solution, valid only for small values of the parameter, St, is available in closed form. The second method of solution (integral) is approximate, but more general than the asymptotic solution. In the integral technique, θ and y^* are essentially eliminated from Equation (5a), and the resulting ordinary differential

equation for S^* as a function of time is readily solved. The third solution method involves the finite difference representation of Equations (5) and is completely general with respect to the form of the boundary conditions at $y^* = 0$ and $y^* = S^*$.

D. Asymptotic Solution for Small Stefan Number

The parameter, St (Stefan number) which arises from the non-dimensionalization of Equation (5a) is an important parameter in determining the way heat is transferred within the solid layer during layer growth. Qualitatively, the Stefan number is often interpreted as a ratio of sensible heat capacity effects to latent heat effects in the layer. If the Stefan number is small, the rate of the solidification or melting process is essentially controlled by the latent heat of fusion, ℓ. In this instance, the temperature profile in the layer will respond more quickly to a change in wall temperature than will the layer thickness and the profile will assume a nearly linear shape throughout the transient. If the assumption of a quasisteady or linear temperature profile in the layer is made, a closed form, analytic solution for the phase boundary position becomes possible.

With the linear assumption,

$$\theta = \frac{y^*}{S^*} \quad . \tag{8}$$

Using this result in the interface heat balance expression, (5f), results in

$$\frac{dS^*}{dt^*} = \frac{St}{S^*} - q^* \quad . \tag{9}$$

If it is assumed further that wall temperature and interface heat flux remain constant, then rearrangement and integration of Equation (9) using condition (5c) yields

$$t^* = \int_1^{S^*} \frac{\eta d\eta}{St - q^*\eta} = \frac{1-S^*}{q^*} + \frac{St}{q^{*2}} \ln \left[\frac{1 - \frac{q^*}{St}}{1 - \frac{q^*S^*}{St}} \right] . \qquad (10)$$

Equation (10) is an expression for the phase boundary position valid for the case of small Stefan number (small heat capacity). The extent to which Equation (10) yields accurate results may only be established by direct comparison with an exact solution for $S^*(t^*)$.

E. Approximate Solution by an Integral Technique

The system, (5), may be solved approximately by estimating the temperature profile in the solid layer with some convenient algebraic expression which satisfies the boundary conditions exactly at $y = 0$ and $y = S$ and the differential equation, (5a), only in the mean [see (14)] for the region $0 < y < S$. Equation (5a) is thereby reduced to an ordinary differential equation for S, the solid layer thickness, as a function of time which may be easily solved by standard techniques.

Integrating Equation (5a) over the solid layer yields:

$$\left.\frac{\partial\theta}{\partial y^*}\right|_{y^*=S^*} - \left.\frac{\partial\theta}{\partial y^*}\right|_{y^*=0} = \frac{1}{St}\frac{dSt}{dt^*}\int_0^{S^*}[\theta-1]dy^* + \int_0^{S^*}\frac{\partial\theta}{\partial t^*}\,dy^* \quad .(11)$$

Interchanging the order of integration and differention in the last term on the right-hand side of Equation (11) and noting that

$$St \left.\frac{\partial\theta}{\partial y^*}\right|_{y^*=S^*} - q^* = \frac{dS^*}{dt^*} \qquad (12)$$

results in:

$$\frac{dS^*}{dt^*} + q^* - St\frac{\partial\theta}{\partial y^*}\bigg|_{y^*=0} = \frac{d}{dt^*}\left[St\left(\int_0^{S^*}\theta dy^* - S^*\right)\right] \quad , \tag{13}$$

which is the basic form of the integral equation for the solid layer.

The form of the algebraic expression chosen to represent the solid layer temperature profile is a second degree polynomial in the dimensionless position coordinate y^*/S^* :

$$\theta = D_1\left(\frac{y^*}{S^*}\right)^2 + D_2\left(\frac{y^*}{S^*}\right) + D_3 \quad . \tag{14}$$

The constants D_1, D_2, and D_3 are chosen so that the temperature profile satisfies the boundary conditions:

$$\theta = 0 \qquad y^* = 0 \tag{15}$$

$$\left.\begin{aligned} \theta &= 1 \qquad (16)\\ St\,\frac{\partial\theta}{\partial y^*} - q^* &= \frac{dS^*}{dt^*} \qquad (17)\end{aligned}\right\} \quad y^* = S^* \quad .$$

Then Equation (14) becomes:

$$\theta = \left[2 - \frac{S^*}{St}\left(\frac{dS^*}{dt^*} + q^*\right)\right]\left(\frac{y^*}{S^*}\right) + \left[\frac{S^*}{St}\left(\frac{dS^*}{dt^*} + q^*\right) - 1\right]\left(\frac{y^*}{S^*}\right)^2 \quad . \tag{18}$$

Substituting Equation (18) into Equation (13) results in:

$$6\left(\frac{St}{S^*} - \frac{dS^*}{dt^*} - q^*\right) = \frac{d}{dt^*}\left[StS^* + \frac{S^{*2}}{2}\left(\frac{dS^*}{dt^*} + q^*\right)\right] \tag{19a}$$

subject to the initial conditions

$$S^* = 1 \qquad \left.\begin{array}{l} \\ \\ \end{array}\right\} \quad t^*=0 \quad . \tag{19b}$$

and

$$\frac{dS^*}{dt^*} = St \left.\frac{\partial\theta}{\partial y^*}\right|_{y^*=S^*} - q^* \qquad \left.\begin{array}{l} \\ \\ \end{array}\right\} \tag{19c}$$

The system, (19), was solved numerically via a fifth-order Runge-Kutta numerical integration formula utilizing Sarafyan embedding for step size control (15).

F. Finite Difference Solution

The finite difference solution of Equations (5) is achieved by employing variable nodal spacing in the solid layer (Figure 2) similar to that used by Murray and Landis (12). This procedure greatly simplifies the solution in the vicinity of the moving phase boundary because the position of the interface always coincides with one of the temperature nodes and interpolation for the phase boundary position becomes unnecessary. In order to develop an equation applicable to the moving nodal point system, the time derivative in (5a), $\partial\theta/\partial t^*$, is expressed in terms of the total time derivative, $D\theta/Dt^*$, and the velocity of the moving nodes, $\frac{y^*}{S^*}\frac{dS^*}{dt^*}$. Thus,

$$\frac{\partial\theta}{\partial t^*} = \frac{D\theta}{Dt^*} - \frac{y^*}{S^*}\frac{dS^*}{dt^*}\frac{\partial\theta}{\partial y^*} \quad . \tag{20}$$

Substituting Equation (20) in Equation (5a) yields,

$$\frac{D\theta}{Dt^*} = \frac{\partial^2\theta}{\partial y^{*2}} - \frac{1}{St}\frac{dSt}{dt^*}[\theta-1] + \frac{y^*}{S^*}\frac{dS^*}{dt^*}\frac{\partial\theta}{\partial y^*} \qquad 0 < y^* < S^* \tag{21a}$$

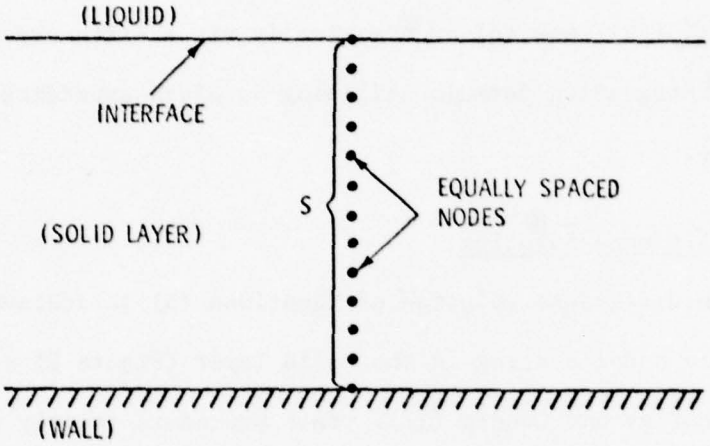

Figure 2. Variable Internodal Spacing in Solid Layer

with the associated conditions,

$$\left.\begin{aligned} \theta &= \theta_o(y^*) \\ S^* &= 1 \end{aligned}\right\} \qquad t^* = 0 \qquad (21b), (21c)$$

$$\theta = 0 \qquad y^* = 0 \qquad (21d)$$

$$\left.\begin{aligned} \theta &= 1 \\ St\,\frac{\partial\theta}{\partial y^*} - q^* &= \frac{dS^*}{dt^*} \end{aligned}\right\} \qquad y^* = S^* \quad . \qquad (21e), (21f)$$

Equation (21a) is solved for the temperature distribution in the solid layer by an explicit forward difference technique. The resulting interfacial temperature gradient $\partial\theta/\partial y^* \Big|_{y^*=S^*}$ is approximated via a three-point backward difference formula and used in condition (21f) to yield the phase boundary velocity and, ultimately, the interface position. The detailed difference equations can be found in Appendix A.

The explicit form of the difference equations simplifies the numerical solution of Equation (21a) considerably; however, with an explicit solution scheme, the question of stability must be considered. According to Özisik (16), there is no general stability criterion for determining the stability limits in nonlinear problems. In most cases, the stability bounds are determined by numerical experiment. In the present study, both the accuracy and stability of the solution are monitored by continuously correcting the temperature distribution and the solid layer thickness at each time step. The corrections are

applied until successive corrections agree to within some specified tolerance. If this criterion is not met after four corrections, the time step is halved and that time step repeated. In all the runs made (over one hundred), there were no instances of instability.

The results of the asymptotic solution for small St, the integral technique, and the finite difference model are illustrated and discussed fully in Chapter IV.

CHAPTER III

EXPERIMENTAL INVESTIGATION

A. Introduction and Purpose of the Experiment

The major objective in carrying out this experimental investigation was to demonstrate the validity and the range of applicability of the general analytical model and numerical solution procedure discussed in Chapter II. The experiment should provide, above all, a means of evaluating the generality of the theoretical model with respect to arbitrary time varying conditions at the solid layer boundaries. On the other hand, the assumption of uni-dimensional heat flow in the solid-layer, and the assumptions that the material in question is a pure substance and that thermodynamic equilibrium exists at the phase change interface must be preserved in the experiment in order to honor the assumptions under which the model was formulated. In particular, the assumption of one-dimensionality is essential to the numerical procedure used in Chapter II to solve the governing energy equation. The variable space node method adopted for this purpose becomes extremely complex if multidimensional heat flow is considered. To the author's knowledge, the variable nodal system has not been implemented in multidimensional phase change problems to date. Thus, the experimental apparatus used in this investigation was designed in such a way as to provide a means of evaluating the theoretical model without violating the basic assumptions under which the problem was formulated.

In order to effect the comparison between experiment and theory, several basic physical measurements must be made with a reasonable degree of accuracy in the experiment. The most important measurements to be made are suggested by Figure 1 and include the local convective heat flux at the solid-liquid interface ($y = S$), the local temperature at the interface between cooling surface and solid layer ($y = 0$), and the local solid layer thickness, S. The first two measurements are the independent or driving variables of the solid layer growth process, while the layer thickness is the resultant of these. Therefore, no effort was expended in the experimental design to provide precise control over the wall temperature, T_w, and heat flux at the interface, q''_c, as long as the variation of each with time could be accurately monitored and recorded. It then becomes a simple matter to use these recorded variations in the analytical model and thus generate theoretical solid thickness variations which may be compared with the experimental results. On the basis of this comparison, the solution procedures set forth in Chapter II can be evaluated.

B. Experimental Apparatus

1. Requirements

The experimental apparatus must, to a reasonable degree, duplicate the conditions shown in Figure 1. Therefore, the geometry chosen for the experiment was that of a plane surface over which the liquid phase could flow in forced convection. The flow regime of the liquid flow past the solid layer was chosen to be one of parallel, turbulent flow. The distinction made here is important because, to the author's knowledge, there has been no other experimental study made of a moving boundary

system which employed turbulent flow at the phase change interface. Also, precautions were taken which would cause the ice layer to remain relatively thin so that heat flow within it would remain essentially one-dimensional. The presumption that the heat conduction in the layer is one-dimensional would be verified experimentally. Provisions also were made to provide a range of heat flux conditions at the interface. This was accomplished by varied liquid temperature and/or liquid flow velocity. The determination of the interface heat flux can be approached from two basic directions. Theories of convection heat transfer may be applied to predict the local film coefficient at a particular point on the solid layer surface, or the heat flux may be determined experimentally using the steady-state solid layer thickness as a form of "heat flux meter." The latter approach is the one adopted here, while convection theory is used to more or less qualitatively verify the results. This approach was taken because the convection heat transfer situation in the experimental apparatus does not correspond very closely to any well-tested heat transfer solution in the literature. Therefore, the experimental approach should prove to yield much more reliable estimates of the interface heat flux and thus provide better information for the analytical model. In addition to a variable interface heat flux, the experimental apparatus must provide a means of varying the solid wall temperature (but not necessarily controlling it). All the primary measurements mentioned in this section must be made dynamically if solid layer growth transients are to be satisfactorily monitored.

2. Basic Configuration

In order to effect the above requirements, a closed flow loop was constructed. The working fluid chosen to be used in the flow loop was ordinary tap water because of its high availability and convenient physical properties (transparency, moderate fusion temperature, etc.). Other fluids were considered, including low melting point eutectic alloys composed of bismuth, lead, tin, and cadmium. However, these materials presented rather substantial difficulties in terms of experimental measurements. The greatest problem being their opaqueness which would make solid layer thickness measurements very difficult. Other disadvantages of the low melting point alloys are their high density, above ambient fusion temperatures, and the extremely high fluidity of these substances in the liquid phase.

The basic components of the flow loop are shown in Figure 3. These consist of various tanks for fluid temperature control, pumps for forced circulation and cooling, a rectangular plexiglas flow channel incorporating the test section and cooling plate, a flow metering device, and the interconnecting tubing. All tubing was made from 2.54 cm (1 inch) inside diameter water hose. The relatively large diameter was chosen in order to minimize pressure loss through the system resulting from the high velocities and volumetric flow rates necessary to insure turbulent flow in the test section. Flow Reynolds numbers used in the experiment ranged as high as 24,000 based upon the flow channel hydraulic diameter. The cooling plate, the leading edge of which was a distance of 64 cm (25.3 inches) downstream of the flow channel entrance, was oriented horizontally and formed the upper wall of the test section. Cooling requirements for the plate were found to be substantial in terms of

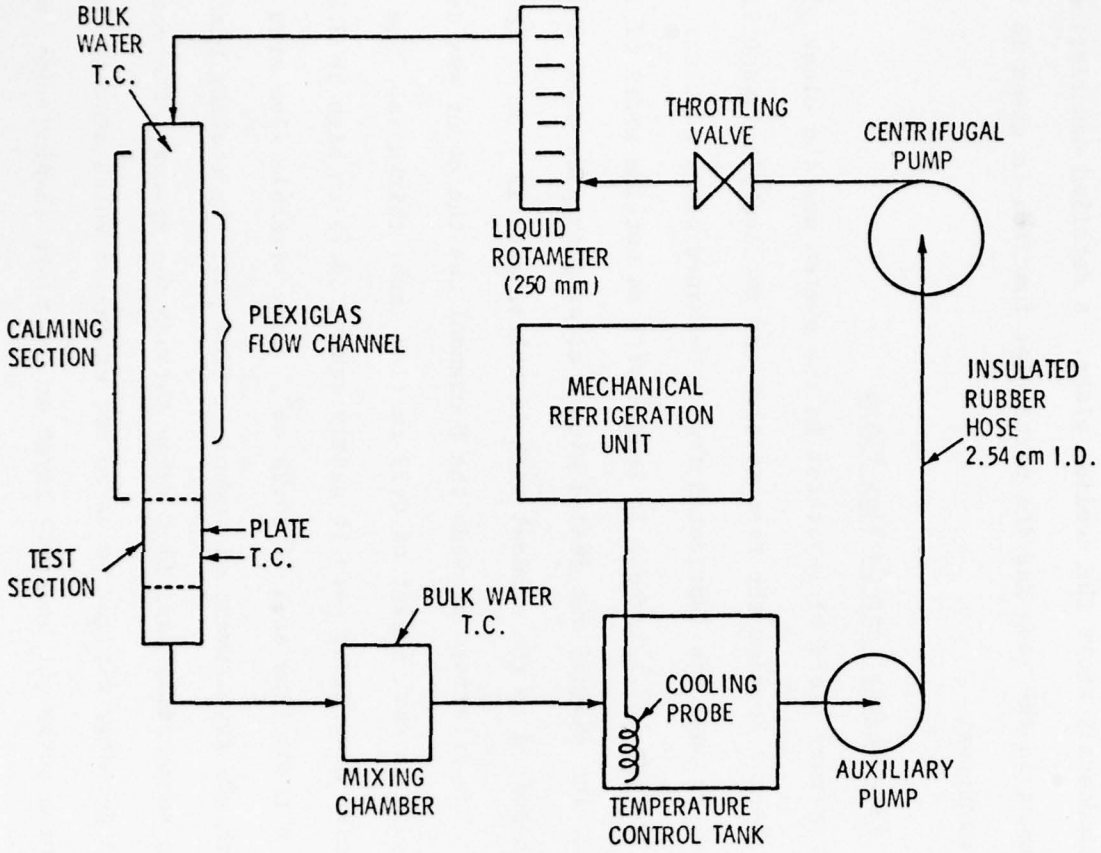

Figure 3. Schematic Diagram of the Experimental Flow Loop

temperature and total heat load due to the very efficient energy transport characteristics of the turbulent channel flow. Cooling of the plate was accomplished totally by means of a dry ice-methyl alcohol bath located immediately above the cooling plate. A detailed description of each component in the loop and its particular function is given in the following sections.

3. Flow Channel and Cooling Plate

The primary piece of apparatus in the system was the clear plexiglas flow channel housing the test section and cooling plate, see Figure 4. The flow channel was fabricated from a U-shaped block of clear plexiglas 92.7 cm (37.5 inches) in length with an outside width of 7.62 cm (3 inches). The channel was sealed with a clear plexiglas cover which was through-bolted to the channel with 18 bolts, each 12.7 cm (5 inches) in length. The interface between the U-channel and the cover was sealed with a multipiece cork gasket of 0.32 cm (1/8 inch) thickness. The channel inside dimensions made it nearly square (3.75 cm high by 3.81 cm wide) with a total flow area of 14.29 cm^2. This sizeable flow area coupled with the requirement of turbulent flow past the cooling plate resulted in substantial mass flow rates through the system. The channel inlet had a geometry similar to an abrupt expansion which assured the existence of a turbulent boundary layer at the plate leading edge even in the low Reynolds number flow ranges. The cooling plate was fabricated from pure copper and was a uniform 0.508 cm (0.20 inches) in thickness. The plate was 18.8 cm (7.4 inches) long in the direction of flow and spanned the entire channel width forming the upper wall of the flow channel. Copper was chosen as the plate material for several reasons.

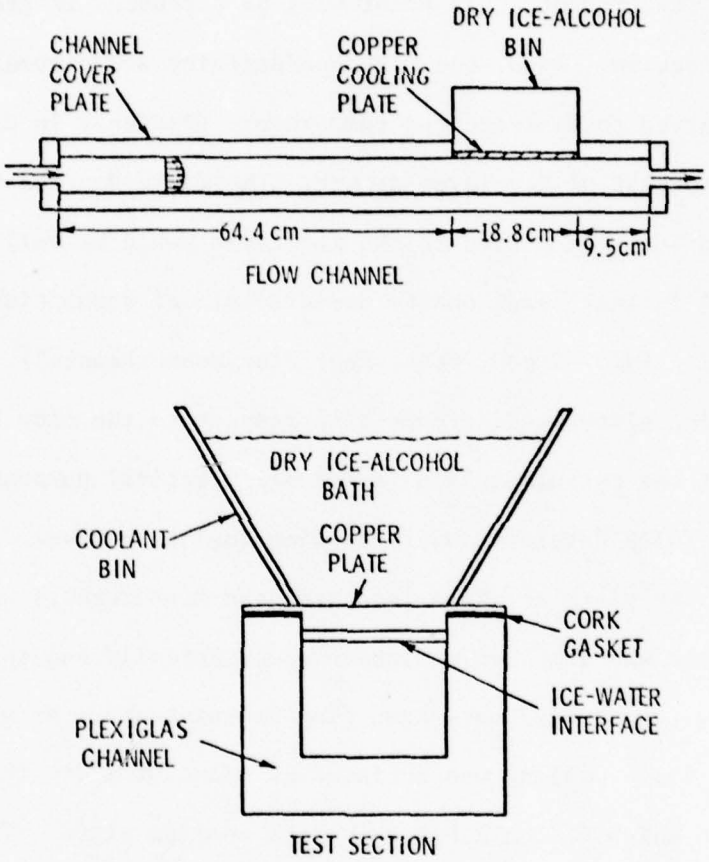

Figure 4. Sketch of the Flow Channel

First, the high thermal conductivity of copper would serve to minimize temperature drop through the plate for a given convective heat flux at the solid-liquid interface. Small temperature gradients through the plate were desirable in order to minimize errors in plate surface temperature measurement, this point will be discussed in greater detail in a later section. Also, the high conductivity and thermal diffusivity of copper served to minimize the temperature gradients in directions transverse to that of ice layer growth. Thus, the desired one-dimensionality of the heat conduction in the ice layer would be very nearly achieved. A further check on the one-dimensional assumption was made experimentally (see "Steady-State Heat Flux Measurements"). The position of the cooling plate leading edge with respect to the flow channel inlet is such that the turbulent flow is for all practical purposes hydrodynamically fully developed where cooling begins; however, at the position on the plate at which ice thickness measurements were made, the boundary layer was somewhat underdeveloped thermally and this fact is confirmed by the steady-state heat flux measurements. As was mentioned previously, plate cooling was achieved by means of a dry ice-methyl alcohol bath which filled a bin above the cooling plate. The bin was fabricated from brass plate which was then silver soldered directly to the upper surface of the cooling plate. The bath had an approximate capacity of 2.5 liters which was found to be sufficient to meet the cooling requirements of the average test run. The bath required no external agitation as sufficient mixing was achieved through the sublimation process of the dry ice itself. On the other hand, it was found necessary to periodically change the alcohol in the bin because it would absorb moisture from the surroundings and, over a period of

time, the water dissolved in the alcohol would affect the ability of the bath mixture to reach sufficiently low temperatures. The plate surface temperature (ice layer side) produced by the bath was in general a function of the rate of heat flow through the cooling plate, which in turn was a function of the ice-water interface heat flux under steady-state ice layer conditions. Visual observation of the ice layer surface and the layer growth process was enhanced by fine polishing the vertical walls of the flow channel in the test section area. Ice layer observation was also improved by back-lighting the test section at an angle which caused light to reflect off the ice layer surface. The entire flow channel, excluding the observation windows in the vicinity of the test section, was thermally insulated with 3.81 cm (1.5 inch) thick polyurethane foam insulation. This heavy insulation assured that the flow upstream of the cooling plate would be uniform in temperature. Thus, channel centerline temperatures measured upstream of the test section would be equivalent to mixed mean fluid temperature. As the water passed through the test section and passed the ice layer, the fluid bulk or mixed mean temperature was considered to remain essentially constant and equal to the inlet temperature due to the relatively small amount of heat transferred to the water per unit mass flowing. This assumption is verified experimentally by measuring the bulk water temperature downstream of the test section. For this purpose, the flow channel and connecting tubing downstream of the test section was also heavily insulated. The entire flow channel assembly was rigidly bolted to a steel frame so that the test section observation windows were supported at an elevation which provided for easy visual inspection of the ice-water

interface. Figure 5 is a photograph of the entire flow channel assembly with the insulation partially removed.

4. Mixing Tank

A cylindrical stainless steel mixing tank was located just downstream of the flow channel exit and test section. The tank, measuring 17.8 cm (7 inches) in diameter and 25.4 cm (10 inches) in length, was baffled so that the water flowing through it would be completely mixed when it reached the tank exit where the water temperature was measured by a thermocouple probe. In this way, a check was made on the assumption that the mixed mean water temperature remained constant through the test section. This tank was also heavily insulated.

5. Temperature Control Tank

Immediately downstream of the mixing chamber was the temperature control tank which was used to remove energy from the working fluid as it flowed around the loop. This tank was open and cylindrical in shape having a diameter of 38.1 cm (15 inches) and normally holding about 26 liters of water. The tank was also insulated with polyurethane foam. It was found that the energy transferred to the water as it flowed through the forced circulation pump exceeded the heat transfer from the water as it flowed past the ice layer. Therefore, a cooling probe was placed in the temperature control tank to remove this excess energy and thus assure that the water would remain at essentially constant temperature throughout a given test. The cooling probe was supplied refrigerant by a mechanical refrigeration unit manufactured by FTS Systems Inc.. The refrigeration system could be operated in one of two modes, constant cooling, or thermostatically controlled cooling in which temperature sensing was

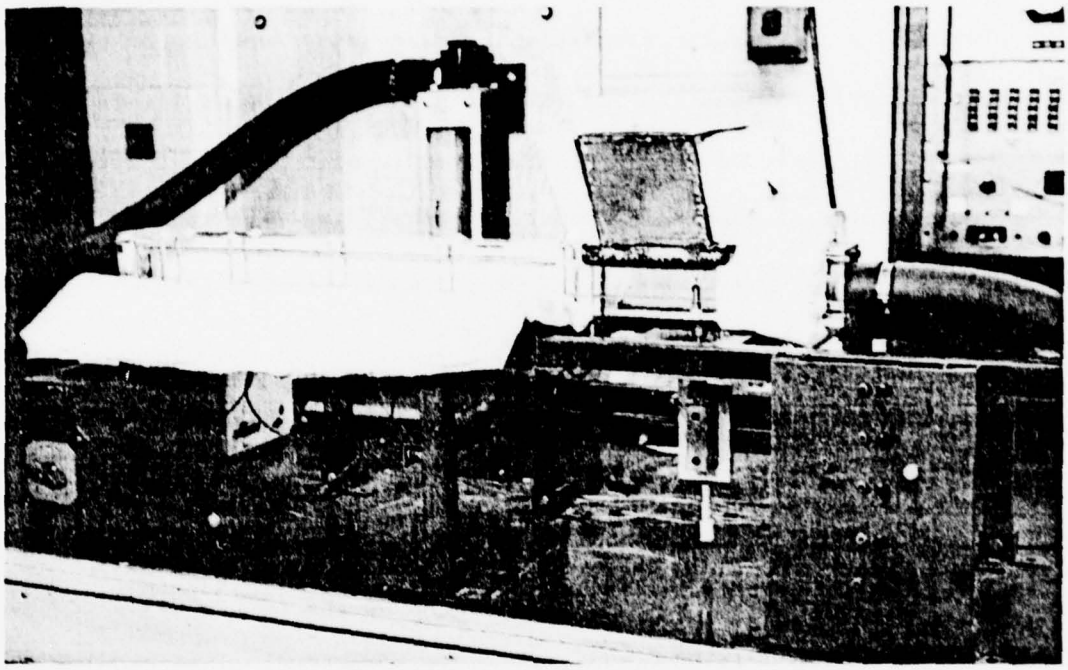

Figure 5. Photograph of the Flow Channel Assembly

achieved through a copper-constantan thermocouple located in the tank. Before a run began, the refrigeration system was used to cool the entire flow loop down to the desired temperature while a small auxiliary pump provided the necessary circulation. A secondary function of the temperature control tank was that of filtering the water as it flowed through the system. Several layers of fine nylon screen covered the tank exit (suction side of the forced convection pump) and thus removed any foreign material from the loop which may have been introduced through the open tank.

6. Forced Circulation Pump

The water flow in the loop was driven by the main pump located somewhat downstream of the temperature control tank. The pump, manufactured by the Allis Chalmers Corp., was of the centrifugal, closed impeller design. It was driven by a 3/4 horsepower close-coupled electric motor. It was found that this combination was capable of providing volumetric flow rates of up to 1.76 liters/sec (28 GPM) and flow velocities of 1.2 m/sec (3.9 ft/sec) corresponding to a flow Reynolds number in the test section of 46,000. The flow rate through the system was controlled by means of a throttling valve on the pump discharge.

7. Flow Meter

Flow measurement was achieved by passing the flow through a 250 mm, high capacity, liquid rotameter manufactured by the Ametek Corporation. The stainless steel float was non-viscosity compensating but did not alter the overall accuracy of the flow measurements because the water temperature range used during steady-state and transient runs represented

a fairly small variation in viscosity. A discussion of rotameter calibration is included in the following section on temperature, flow, and ice thickness measurements.

C. Temperature, Flow, and Ice Thickness Measurements

As mentioned previously, the two primary temperature measurements made in the experimental investigation were the cooling plate surface temperature and bulk water temperature. The plate surface temperature in the immediate vicinity of the ice thickness measurement was used in forming the dimensionless parameter, $St = c(T_m - T_w)/\ell$, while the bulk water temperature was used indirectly in determining q''_c, the heat flux at the ice-water interface required to compute the dimensionless heat flux parameter, $q^* = q''_c \, S_o/\ell\rho\alpha$.

1. Temperature Measurement

Cooling plate surface temperatures were obtained from two thermocouples imbedded in the plate just below the plate surface, immediately upstream and downstream of the location where ice thickness measurements were made. The copper-constantan thermocouple wires were 0.072 mm (0.003 inch) in diameter and were insulated by a teflon coating. The copper-constantan wire combination was chosen for the plate thermocouples because wires made from these materials are normally of a high degree of homogeneity and, therefore, temperature gradients existing along the wires do not cause the generation of extraneous EMF's within the thermocouple circuit. The two wires of each thermocouple were laid side-by-side in two shallow grooves which were machined into the surface of the copper cooling plate as shown in Figure 6. Each groove was 0.76 mm deep and 1.02 mm in width and extended from the edge of the plate to slightly over

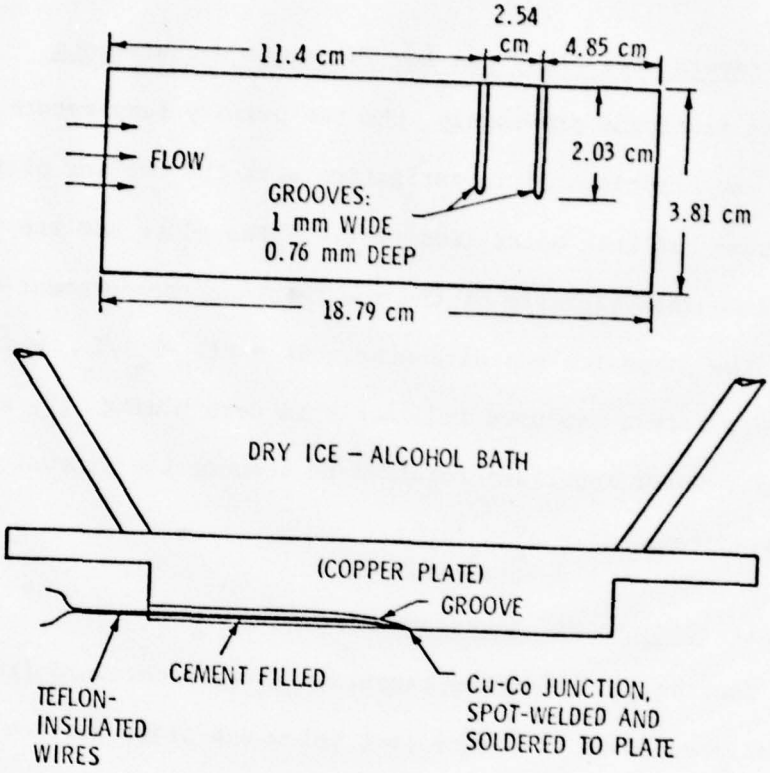

Figure 6. Diagram Illustrating the Method of Plate Surface Temperature Measurement

halfway across it, perpendicular to the direction of flow. At the end of each groove the "floor" of the groove sloped downward to meet the plane of the plate surface in a gradual manner, see Figure 6. This configuration allowed the junction of the thermocouple to lie very near to the plate surface. The junction itself was made by a small spot weld at the wire ends. The welded junction was soldered to the plate at the end of the groove. The excess solder was filed off level with the plate surface and then polished smooth with a fine abrasive. The remainder of the open groove between the thermocouple junction and plate edge was filled in with cement and sanded smooth and level with the plate surface. The problem normally associated with accurate surface temperature measurement, that of maintaining thermal equilibrium between the thermocouple junction and the surface, was minimized in this instance by the high thermal conductivity of the copper from which the cooling plate had been fabricated. Measured heat fluxes through the plate in the direction perpendicular to the plate surface indicate that steady state temperature gradients in the plate, in this normal direction, were a maximum of about 1.5° C/cm. Therefore, errors in surface temperature measurement were not considered to be large because the total temperature drop through the cooling plate was less than 1° C. However, in order to verify that the overall error involved in the plate surface temperature measurement was indeed small, the following check was used. A thin ice layer was grown over the entire cooling plate surface by adjusting the convective heat flux at the ice-water interface through manipulation of the water flow rate in the channel. The convective flux was then increased slowly by increasing the water flow in small increments until the temperature of the extreme upstream edge of the plate rose above the fusion temperature.

This resulted in the downstream portion of the plate being covered by a thin patch of ice. As flow rate was increased still further, the forward edge of the ice patch moved downstream toward the surface temperature measurement positions. As the edge of the patch reached and crossed over these locations, the thermocouple junction outputs were monitored on a strip chart recorder so that the measured surface temperature could be compared with the actual surface temperature (assumed to be 0°C, the fusion temperature) at the precise instant at which the ice patch "uncovered" the surface thermocouples. This procedure was repeated several times for each of the two surface thermocouples. The results showed that each thermocouple measured temperature consistently to within 0.25°C of 0°C. The assumption made here that the actual surface temperature was 0°C is supported by the findings of Siegel and Savino (7), in which the temperature of the ice-water interface under similar experimental conditions was always found to be within 0.1°C of 0°C.

Each wire of the two copper-constantan thermocouples was run out of the flow channel through grooves in the cork gasket which was installed between the upper surface of the flow channel and the copper plate. Both thermocouples were referenced at 0°C with a "Frigistor" automatic ice point reference junction. The two plate surface thermocouple outputs could be read by strip chart recorder or through an integrating digital voltmeter, or both.

Bulk water temperatures were measured with chromel-constantan thermocouple probes located 25.4 cm (10 inches) upstream of the cooling plate leading edge and also downstream of the test section in the mixing chamber. The upstream probe was of the exposed junction type and extended through the floor of the flow channel so that the junction was located

approximately at the geometric center of the channel cross sectional flow area. The centerline fluid temperature indicated by the probe was taken to be identical with the bulk fluid temperature at the upstream end of the test section because of the heavy insulation which covered the flow channel and inlet piping. Errors in bulk water temperature measurement due to heat conduction along the stainless steel thermocouple probe sheath were considered negligible for several reasons. First of all, the overall temperature difference between the surrounding atmosphere and the flowing water was always less than 15°C; thus, there was little driving potential for heat conduction along the probe sheath. Also, the base of the probe was threaded into the plexiglass flow channel which in turn was heavily insulated. Therefore, the flow channel and, hence, the base of the probe could not have been at a temperature significantly different from that of the water, reducing even further the potential for heat flow. Finally, the water flow velocities through the flow channel (0.35 m/sec. to 0.60 m/sec.) would produce heat transfer coefficients over the probe of such a magnitude that heat conducted to the probe junction (possibly through the thermocouple lead wires) would be efficiently transferred to the flowing water through a very small temperature difference.

The downstream probe was used primarily to verify that the bulk water temperature remained essentially constant as it passed through the test section. This chromel-constantan probe was of the grounded-junction type and extended about 7.6 cm (3 inches) into the mixing chamber. For reasons similar to those outlined above, conduction error was also considered negligible in the temperature measurements made with this probe. Both bulk water temperature thermocouple probes were referenced

at 0°C with the Frigistor automatic ice point reference. The outputs of each probe could be read from a digital voltmeter or continuously monitored by strip chart recorder. The maximum uncertainties involved in the measurement of bulk and plate surface temperatures (including uncertainties due to the limited reading precision of the strip chart recordings) were estimated as 0.5°C and 0.2°C for the plate and bulk water temperature measurements, respectively.

2. Flow Measurement

Water flow rate measurement in the test loop was achieved with a standard liquid rotameter with a 250 mm meter tube. The rotameter float was of the non-viscosity compensating or streamlined type; however, this did not significantly affect flow measurement accuracy because bulk water temperatures varied only over a small range during the experiments (less than 10°C). The rotameter was calibrated directly with tap water at temperatures within the range used in both steady-state and transient experiments. The 36-point calibration yielded a calibration curve which fit the 36 data points with a root mean square deviation of 0.43 liters/min. for volumetric flows between 18.9 liters/min. and 104 liters/min. The accuracy with which the flow rate could be measured depended also upon the degree of precision to which the instrument could be read. This was not a limiting factor in the present study because the flute-guided meter tube allowed the float position to be estimated to within $\pm$ 1 mm ($\pm$ 0.40 liters/min.) under most circumstances. Some degree of float oscillation did occur at low flow rates; under these conditions, the mean flow rate was considered to correspond to the midpoint of the total range of float oscillation. The absolute maximum uncertainty in the flow measurements

was estimated as $\pm$ 0.87 liters/min. (corresponding to the largest deviation of the data from the fitted calibration curve) which represents three percent of the lowest flow rate encountered in any part of the experiment.

3. Ice Layer Thickness Measurement

Accurate measurement of the thickness of the ice layer which formed on the copper cooling plate, both at steady-state and under transient conditions, was essential in the experimental investigation. There are a number of ways in which the measurement can be made, all of which fall into basically two categories: optical methods, and mechanical probe methods. A short discussion of the measurement techniques of each type follow.

a. Optical Measurement Techniques

The ice layer thickness can be measured by photographing the ice layer in a direction normal to the water flow and in the plane of the ice-water interface as shown in Figure 7. The photographs taken in this manner are then enlarged and the ice layer thickness is determined from the enlargements. This method was one of those used by Siegel and Savino (7) in an experimental study similar to the present one. From the figure, it is seen that this method of ice thickness measurement is useful only when the ice layer is of fairly constant thickness across the channel. The photographic method yields measurements of the thickest portion of the ice layer and cannot be used to measure a "point thickness" at some specific location on the plate. Other factors which limit the accuracy of the photographic technique, according to Siegel and Savino, are optical distortion effects, optical illusions, difficulties in obtaining

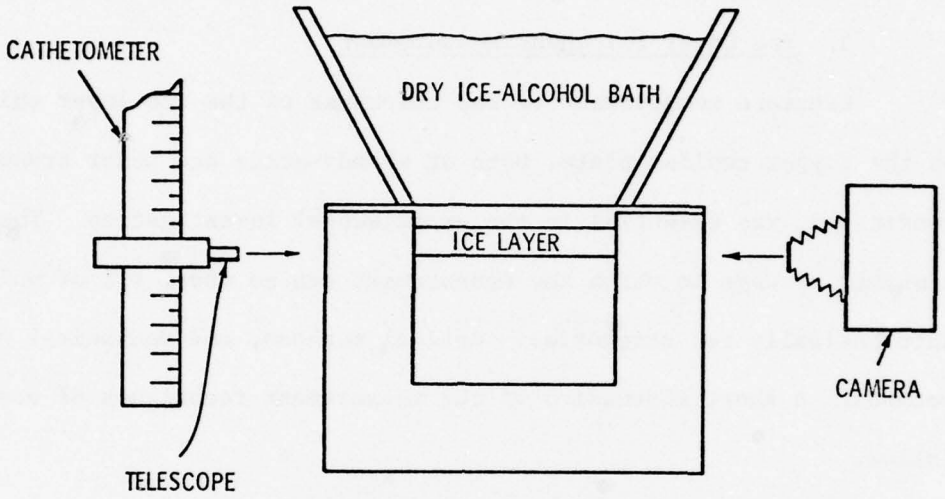

Figure 7. Illustration of the Photographic and Cathetometer Ice Thickness Measurement Techniques

exact camera alignment with the plane of the ice interface, and limited image magnification. Optical distortions resulted from the temperature gradient in the thermal boundary layer immediately adjacent to the interface, and optical illusions arose due to the transparency of the ice layer surface. Image magnification was a problem despite the use of a 70 mm camera in the Siegel and Savino study. Transient ice growth measurement by the photographic technique involved special difficulties in that the camera alignment with the ice-water interface had to be continuously adjusted throughout the transient.

A second optical method of ice thickness measurement, also discussed by Siegel and Savino, is achieved by visual means rather than photographic. This measurement technique is also illustrated in Figure 7, in which a small telescope mounted on a cathetometer is used to visually locate the ice-water interface. With this method, grids of horizontal lines spaced at a known distance apart are placed on both walls of the flow channel. When the interface is sighted with the telescope in the same plane as two corresponding grid lines on either side of the channel, the ice layer thickness is simply read from the grids. According to Siegel and Savino, this technique was found to suffer from many of the same disadvantages as the photographic method; i.e., optical distortion due to temperature gradients in the boundary layer and difficulties in locating the transparent ice surface.

Neither of the optical methods described above are ideal for measurement of solid layer thicknesses at a specific point on the cooling plate. The mechanical and temperature probe methods described below do not have this limitation.

b. Mechanical and Temperature Probe Techniques

The mechanical probe method of ice thickness measurement consists of introducing a small probe into the test section through the channel wall opposite the ice layer and raising the probe until it contacts the layer surface, thus yielding a direct measurement of the ice layer thickness at a given point on the cooling plate. A variation of this procedure was used by Siegel and Savino in which the probe was fabricated in the form of a fine gauge, forked thermocouple probe, see Figure 8. The thermocouple wire extending between the fork-like supports was 0.076 mm (0.003 inch) in diameter with a butt-welded junction at the center. The probe shaft was mounted in a micrometer head so that it could be raised or lowered in fine increments. In measuring the ice layer thickness, the probe was made to approach the ice surface slowly while monitoring the output of the probe thermocouple on a strip chart recorder. When the thermocouple output corresponded to 0°C, the fusion temperature, the probe was assumed to be in contact with the ice layer surface and the thickness was then read from the micrometer dial. According to Siegel and Savino, this temperature probe method of ice thickness measurement proved to be most accurate and was reported to yield thickness measurements correct to within 0.025 mm (0.001 inch). In addition to the temperature probe, a purely mechanical probe was also employed in the Siegel and Savino experiments to measure ice layer thickness under steady-state conditions. This probe consisted of a thin metal rod which was mounted in a micrometer head in a manner similar to the temperature probe. The rod was moved toward the interface until it was visually determined that the probe had contacted the ice layer, at which time the ice thickness was read from the micrometer. It was not stated by the authors to what degree of accuracy

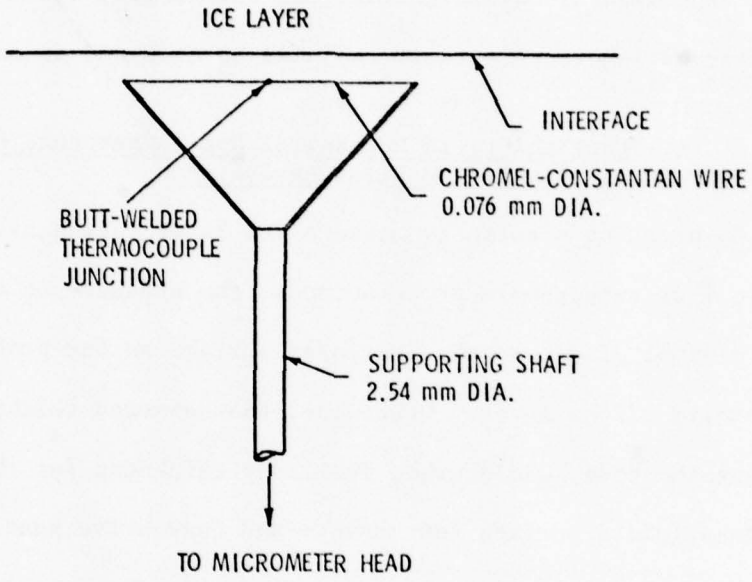

Figure 8. Illustration of the Thermocouple Probe Ice Thickness Measurement Technique

the ice thickness could be measured by this method. Both the temperature and mechanical probe methods described here raise significant questions with respect to their accuracy in the experimental determination of ice layer thickness. Because a similar type of ice probe was used in the present experimental investigation, the advantages, disadvantages, and uncertainties inherent in their use will be examined in some detail.

c. Uncertainty in Mechanical and Temperature Probe Techniques and Simplified Error Analysis

In order to accurately measure ice layer thickness by either mechanical or temperature probe methods, the presence of the probe must have a minimal effect on the ice layer surface as the probe is moved into the vicinity of the layer. Otherwise, the measured thickness will not represent the true, undisturbed ice layer thickness for the prevailing conditions (plate surface temperature and convective heat flux at the interface). The phenomenon under consideration here is somewhat analogous to the so-called "loading error" which may occur in electrical, transducer-type measurement devices. The fundamental principal which governs in both instances is that the measurement process will inevitably alter the quantity which is to be measured, see Reference 17. Errors of this type arise in mechanical probe thickness measurements primarily because the probe must be of finite dimension and therefore, when brought into the immediate vicinity of the ice-water interface, will have some effect on the convective heat transfer phenomena occurring there. The effect probably can be attributed to a local flow distortion caused by the probe's presence which in turn perturbs the local convective heat flux at the ice-water interface from its "normal" (in the absence of the probe) value. This flow distortion effect will always be present to some degree and its

magnitude will probably depend heavily on the probe size and shape in addition to the flow conditions at the interface. In the present experimental study, the ice thickness always tended to decrease very slightly in the extended presence of the probe, thus implying a slightly increased heat transfer coefficient at the interface. To minimize the distortion of the ice layer due to the probe, steps may be taken in the design of the probe and also in the experimental technique.

Ice thickness measurement by the temperature probe method similar to that used by Siegel and Savino is subject to an even wider range of experimental errors. In addition to the requirement that the probe should not disturb the ice-water interface, the basic principal of the measurement technique requires that the probe tip or thermocouple junction be very nearly in thermal equilibrium with its surroundings when the junction is immediately adjacent to the ice layer surface. In other words, the conduction error must be kept small if accurate ice thickness measurements are to be made. In order to gain a better qualitative understanding of the immediate conduction error problem and to identify the effects of probe size, bulk water temperature, flow conditions, etc., a simplified analysis was carried out for a cylindrical probe projecting into the thermal boundary layer adjacent to the solid-liquid interface.

Consider the situation shown in Figure 9. The cylindrical probe of diameter "d" projects perpendicularly into the thermal boundary layer and virtually contacts the ice-water interface. For the purposes of this analysis, it was assumed that heat is transferred to or from the probe tip by forced convection. The water which flows past the probe and over the interface is assumed to flow under the influence of a negligibly small pressure gradient and with thermal and hydrodynamic boundary layer

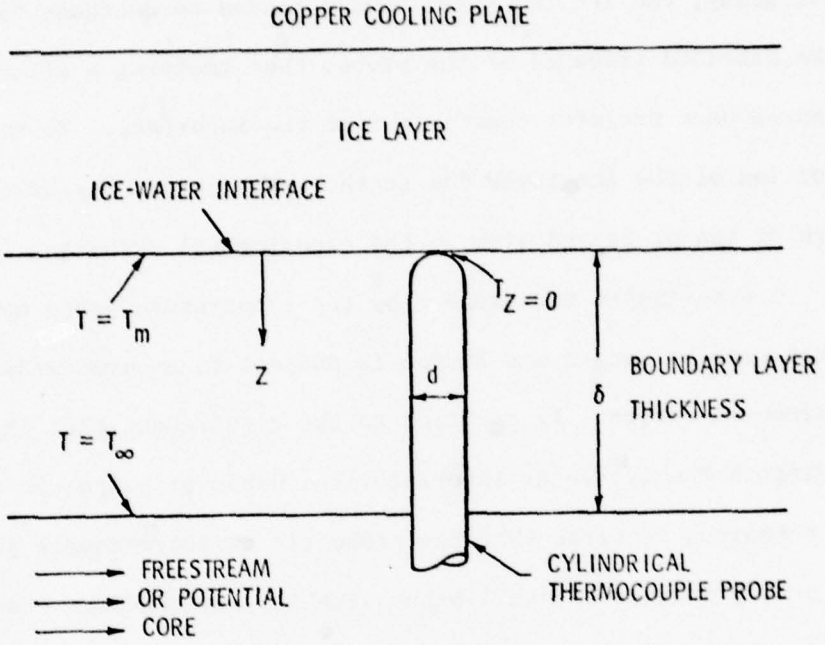

Figure 9. Sketch Showing the Thermocouple Probe Immersed in the Thermal Boundary Layer

thicknesses of comparable dimension ($\delta_h \simeq \delta_t = \delta$). Further simplifying assumptions made in the analysis are listed below.

1. Conduction heat transfer within the probe is one-dimensional and in the direction perpendicular to the ice layer surface (the probe has an effective thermal conductivity in this direction of "λ").
2. At the outer edge of the thermal boundary layer $Z = \delta$, the probe temperature corresponds to that of the freestream, T_∞.
3. The fluid temperature in the boundary layer (T_F) varies with Z from the melting temperature (T_m) at $Z = 0$ to the free-stream temperature (T_∞) at $Z = \delta$. The specific dependence of T_F on Z will be discussed after developing the model.
4. In the interval $0 < Z \leq \delta$, a uniform, average film coefficient exists over the probe surface of magnitude $\bar{h}$.
5. The tip of the probe transfers heat to or from the fluid via the effective film coefficient h_t which is based upon the temperature difference ($T_{Z=0} - T_m$).

The validity of the uniform film coefficient assumption probably depends upon the magnitude of the actual variation of the conductance in the interval $0 < Z \leq \delta$. If this variation is small, the assumption of uniformity in the film coefficient should not introduce significant error into the analysis. It is shown below that the local film coefficients at any two points on a small diameter probe in a low speed flow are of the same order of magnitude.

Consider the crossflow of a liquid over the cylindrical probe shown in Figure 10. For $10 < \text{Re}_d = {}^{Vd}/\nu < 1000$, the boundary layer over much

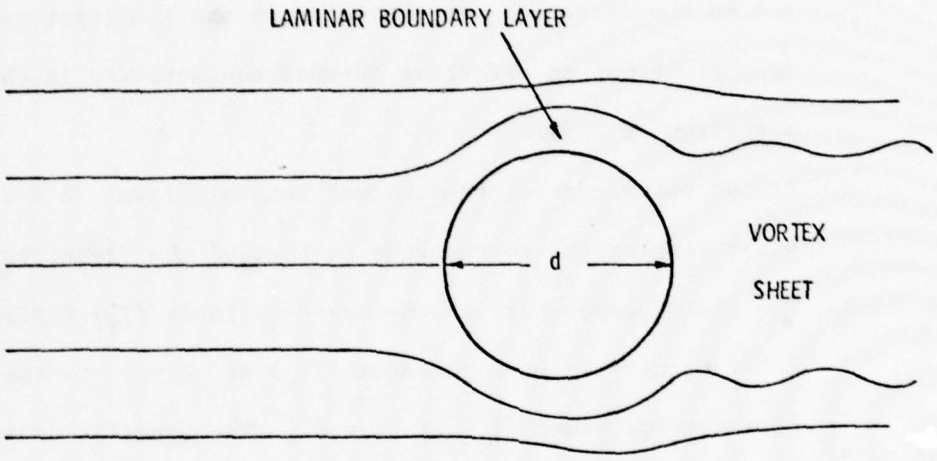

Figure 10. Sketch of the Laminar Boundary Layer on a Cylinder in Crossflow at Low Red

of the probe periphery is laminar with small vortices being shed in the vicinity of the downstream stagnation point (Reference 18). Within this range of Red, the character of the boundary layer flow and therefore the heat transfer phenomena on the cylinder do not change significantly with Red. Thus, it is expected that Nud for this Red range is not a strong function of Red. For the flow conditions encountered in the experimental apparatus described earlier, the maximum value of Red was always less than 200 based on the freestream velocity. From the above considerations, it can be concluded that a largely laminar boundary layer exists over the probe for all values of Z between $Z = 0$ and $Z = \delta$ providing an essentially uniform film coefficient over the entire probe. The variation of viscosity between $Z = 0$ and $Z = \delta$, also reduces the variation in h along the probe shaft. As Prandtl number increases at constant Red, Nud increases at a rate of approximately $Pr^{1/3}$. For example, consider the correlation due to McAdams (18) for liquids in crossflow over cylinders,

$$Nud = 1.1(Red)^{n} Pr^{0.31} . \tag{22}$$

It was determined from this equation and from typical property values and flow conditions encountered in the present experiment that Nud varied by a factor of about 2 between two positions on the probe for which Red varied by an order of magnitude. Therefore, the uniform film coefficient assumption is reasonable, at least for the level of analysis to be carried out here.

With these assumptions, an energy balance on a differential element of the probe yields the following simple system:

$$\frac{\lambda d^2}{4}\frac{d^2T}{dZ^2} - \bar{h}d(T-T_F) = 0 \qquad 0 < Z < \delta \qquad (23a)$$

$$T = T_\infty \qquad Z = \delta \qquad (23b)$$

$$\lambda \frac{dT}{dZ} - h_t(T-T_m) = 0 \qquad Z = 0 \ . \qquad (23c)$$

By introduction of the dimensionless quantities,

$$\Delta = \frac{T-T_m}{T_\infty - T_m} \qquad \text{and} \qquad Y = \frac{Z}{\delta} \ ,$$

and substitution into Equations (23), the following dimensionless system results:

$$\Delta'' - \gamma^2\Delta = -\gamma^2\Delta_F \qquad 0 < Y < 1 \qquad (24a)$$

$$\Delta = 1 \qquad Y = 1 \qquad (24b)$$

$$\Delta' - \beta\Delta = 0 \qquad Y = 0 \ . \qquad (24c)$$

The parameters γ and β are given by,

$$\gamma^2 = \frac{4\bar{h}}{\lambda d}\delta^2 \qquad (25)$$

$$\beta = \frac{h_t\delta}{\lambda} \ , \qquad (26)$$

while Δ_F is the dimensionless local fluid temperature in the boundary

layer,

$$\Delta_F = \frac{T_F - T_m}{T_\infty - T_m} \quad . \tag{27}$$

For a given boundary layer thickness, γ^2 and β indicate the magnitudes of the film coefficients over the probe shaft and probe tip, respectively. The deviation from zero of $\Delta(0)$, the dimensionless probe tip temperature, is a direct indication of the amount by which the tip temperature differs from the melting temperature, T_m, and hence, is a measure of the conduction error which would affect the accuracy of the measurement. The general solution to the system (24) is given by Equation (28).

$$\Delta(Y) = A\sinh \gamma Y + B\cosh \gamma Y - \gamma \int_o^Y \Delta_F \sinh \gamma(Y-\eta)\, d\eta \quad , \tag{28}$$

where the constants A and B are obtained from conditions (24b) and (24c):

$$A = [\frac{\beta}{\gamma} + \beta \int_o^1 \Delta_F \sinh \gamma(1-\eta)\, d\eta]/[\frac{\beta}{\gamma} \sinh \gamma + \cosh \gamma] \tag{29}$$

and

$$B = [1 + \gamma \int_o^1 \Delta_F \sinh \gamma(1-\eta)\, d\eta]/[\frac{\beta}{\gamma} \sinh \gamma + \cosh \gamma] \quad . \tag{30}$$

The temperature profile in the boundary layer $T_F(Z)$ has a substantial effect on the probe tip temperature. Therefore, three temperature profiles will be considered here, two of which correspond to the commonly encountered hydrodynamic regimes of laminar and turbulent boundary layer flow. The temperature variations in the boundary layer were taken to be the same as those commonly employed in the thermal

analysis of two-dimensional boundary layers via the energy integral equation. Each profile can be expressed by:

$$\Delta_F = C_1 Y + C_2 Y^{\kappa} \quad , \tag{31}$$

where the values of the constants C_1, C_2, and κ in Equation (31) for the linear, laminar, and turbulent temperature profiles are shown in Table 1 (Reference 19 and Reference 14). The profiles are also plotted in Figure 11.

Substitution of the linear profile into Equations (28), (29), and (30) results in the following simple relationship between Δ and Y :

$$\Delta(Y) = Y + \frac{\sinh\gamma(1-Y)}{\gamma\cosh\gamma + \beta\sinh\gamma} \quad . \tag{32}$$

The dimensionless probe tip temperature becomes:

$$\Delta(0) = \frac{1}{\gamma\coth\gamma + \beta} \quad . \tag{33}$$

Note that $\Delta(0)$ tends toward zero when γ and/or β become large. Thus it is possible, at least in the case of a linear temperature profile, to decrease the difference between the probe tip temperature and the melting temperature by increasing the film coefficients over the probe shaft and/or probe tip.

For the laminar and turbulent temperature profile, $\Delta(Y)$ was obtained through numerical integration of Equation (28) via Simpson's 3/8 rule. The results are shown in Figures 12 and 13.

TABLE 1

Coefficients C_1, C_2, and κ in Equation (31)

Profile	C_1	C_2	κ
Linear	1	0	-
Laminar	3/2	-1/2	3
Turbulent	0	1	1/7

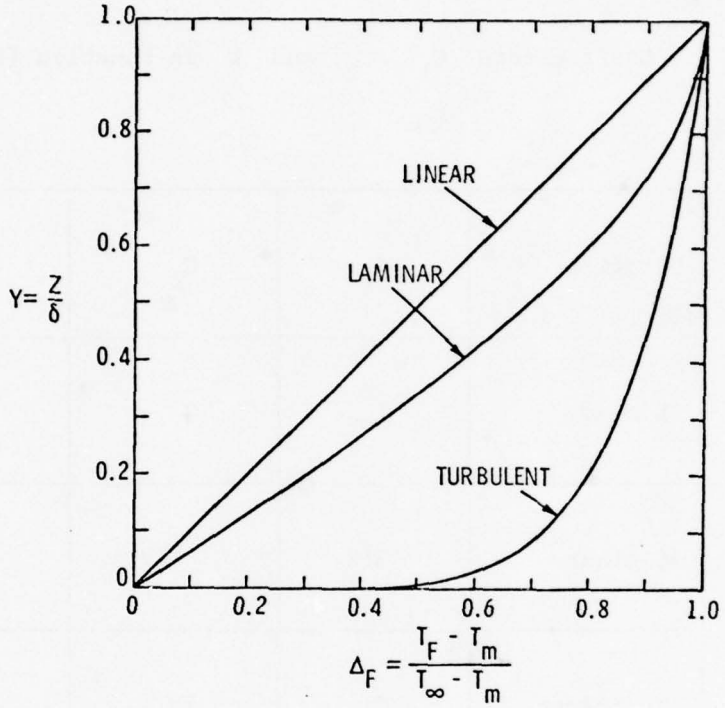

Figure 11. Linear, Laminar, and Turbulent Boundary Layer Temperature Profiles

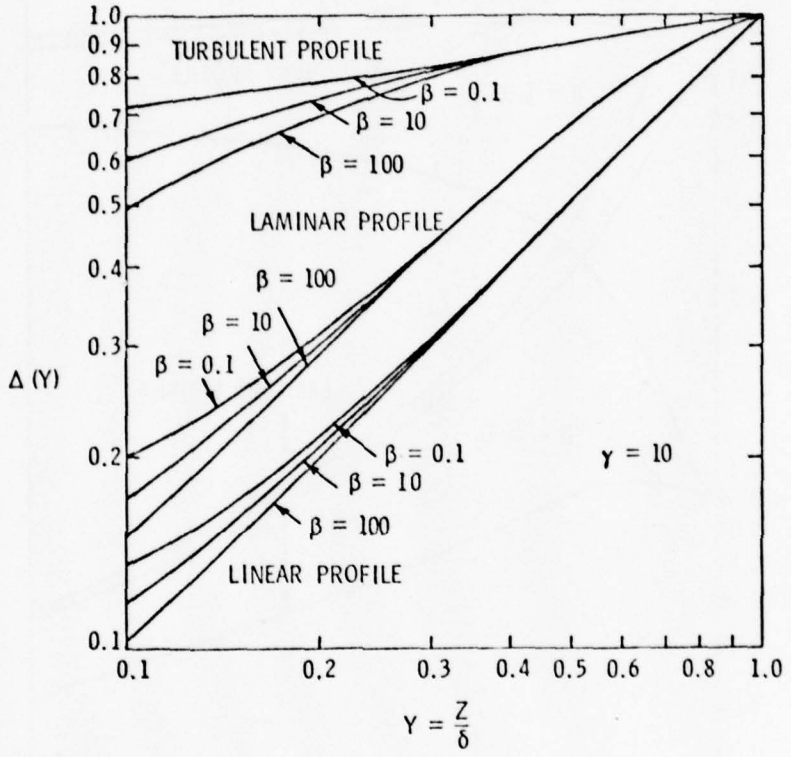

Figure 12. Dimensionless Probe Temperature Δ, Versus Y

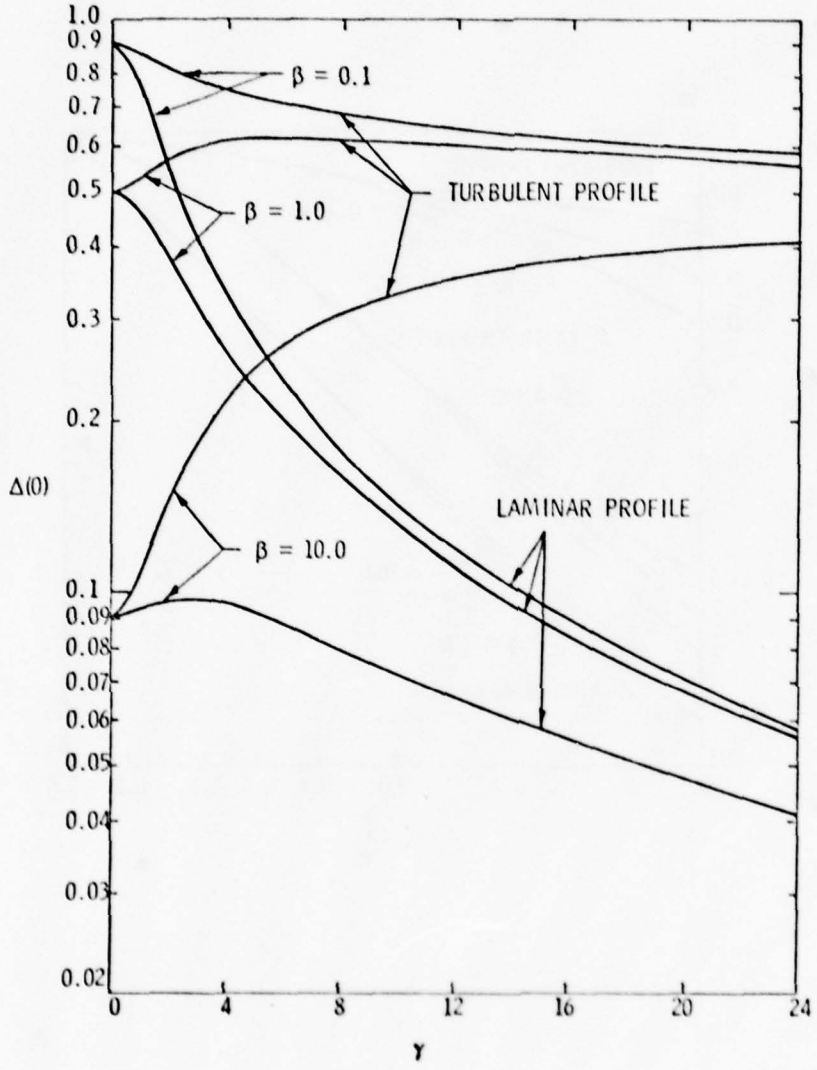

Figure 13. Variation of $\Delta(0)$, the Dimensionless Probe Tip Temperature, with γ

Figure 12 is a plot of the dimensionless probe temperature, Δ, as a function of Y for all three temperature profiles with β as a parameter and $\gamma = 10$. From this figure, there is seen to be a substantial variation in probe temperature due only to differences in the boundary layer temperature profile, all other conditions held constant. Also, the effect of increased film conductance at the probe tip or increased thermal boundary layer thickness (increased β) serves to decrease the dimensionless probe temperature for small values of Y. For Y values approaching unity, the convective boundary condition at $Y = 0$ has little effect and Δ is seen to approach Δ_F, the local boundary layer fluid temperature (compare with Figure 11). This behavior for the laminar and turbulent boundary layer profiles parallels that found in Equation (32) for the linear profile.

The critical quantity with regard to thermocouple probe measurements of ice layer thickness is $\Delta(0)$, the dimensionless probe tip temperature. A zero value of $\Delta(0)$ indicates that the probe tip is at the same temperature as the ice-water interface. In reality, however, $\Delta(0)$ can only approach zero if the probe tip remains in the position shown in Figure 9. The tip temperature can be made equal to the melting temperature only by advancing the warm probe tip into the ice layer, thus distorting the layer surface and yielding false thickness readings. The magnitude by which $\Delta(0)$ deviates from zero when the tip is immediately adjacent to the undeformed layer is shown in Figure 13. The significance of the boundary layer temperature profile is readily obvious from the curves in this figure. For all values of the parameter β shown, the values of $\Delta(0)$ indicated for the laminar and turbulent boundary layer temperature profiles differ by nearly an order of magnitude for values of

the parameter γ greater than about 20. For low values of γ, the curves for the laminar and turbulent profiles converge and eventually meet at $\gamma = 0$. The coincidence of the curves at $\gamma = 0$ derives from the fact that the probe is perfectly insulated for $\gamma = 0$ and $\Delta(0)$ is therefore independent of temperature variations in the boundary layer. A somewhat surprising feature of the curves in Figure 13 is that $\Delta(0)$ is not necessarily a monotonically decreasing function of γ. For large values of the probe tip film coefficient h_t (large values of β), $\Delta(0)$ increases for a time with increased $\bar{h}$ (increased γ) and then decreases toward zero for larger values. This effect is seen to be especially pronounced in the case of a turbulent boundary layer temperature profile. In fact, for turbulent profiles and values of $\beta > 1$, conduction error could probably be more effectively reduced by insulation of the probe shaft. If the shaft is not insulated, then to decrease the conduction error, γ (or $\bar{h}$) must be increased to a value to the right of the maximum in the $\Delta(0)$ curve. In order to attach some physical significance to this effect, consider Figure 14 in which the probe is shown schematically along with the turbulent fluid temperature profile. For $\gamma = 0$ (probe shaft insulated), the probe is in thermal communication with the surrounding fluid only at the tip $(Y = 0)$ via the dimensionless conductance β and the temperature profile in the probe is linear. For very large β, the tip temperature will approach $\Delta(0) = 0$. If γ is increased to some small, non-zero value, the tip area of the probe $(Y = 0)$ will be exposed to the fluid temperature Δ_F which increases very rapidly for small Y and heat will be transferred to the probe from the fluid by convection and then flow toward the tip, thus, increasing the tip temperature. As γ is increased further (moving toward the right on

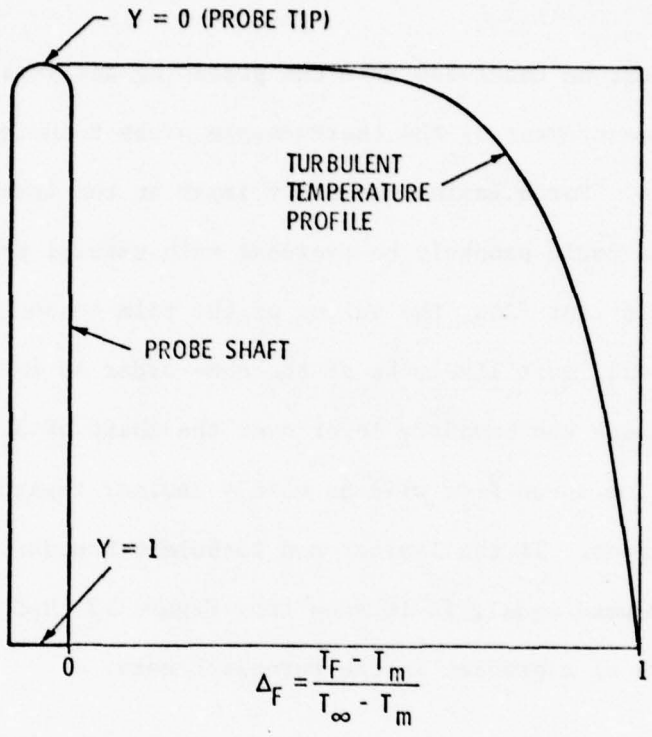

Figure 14. Sketch of Thermocouple Probe and Turbulent Temperature Profile

Figure 13), this effect must eventually reverse itself because, for infinite shaft conductance ($\gamma \to \infty$), the temperature profile in the probe will coincide with the temperature profile in the fluid, and then $\Delta(0) = 0$.

It must be concluded from the preceding analysis that ice layer thickness measurement by the thermocouple probe technique poses many difficulties. For a laminar boundary layer at the ice-water interface, the problems could probably be overcome with careful probe design and use. In turbulent flow, the values of the film conductance parameters γ and β will most likely be of the same order as in laminar flow. This is because the boundary layer over the shaft of a small diameter probe in a low speed flow will be mainly laminar regardless of surrounding flow conditions. If the laminar and turbulent boundary layer thicknesses are also assumed equal, it is seen from Figure 13 that conduction error is much more of a problem in the turbulent case.

d. The Method Used in this Study

It has been shown that the difficulties in obtaining ice layer thickness measurements with the thermocouple probe technique are substantial. In addition, the problems were shown to be far more serious when the boundary layer flow at the ice-water interface is turbulent rather than laminar. For these reasons, a thermocouple probe technique was not used in this study to measure ice layer thickness. All steady-state and transient thickness measurements were made by means of a mechanical probe method in which the probe tip was allowed to just contact the ice layer. Contact between probe tip and ice layer was verified visually by means of a large magnifying lens mounted outside of

the test section. The probe used was a thermocouple probe; however, the thermocouple feature of the probe was not used to directly measure ice layer thickness but only to aid in the recording of transient ice thicknesses.

The thermocouple probe was stainless steel sheathed, cylindrical, and had an overall diameter of 0.25 mm (0.01 inch). The thermocouple junction was made from 0.04 mm (0.0015 inch) diameter chromel and constantan wires and was grounded to the probe sheath at the tip. The fine gauge probe was supported by two larger, concentric stainless steel tubes which projected through the floor of the flow channel below the cooling plate. The larger tube was 0.635 cm (0.25 inch) in diameter and 15.24 cm (6 inches) in length. This shaft was secured to the slider block of a "Unislide" micrometer mechanism mounted underneath the test section. The "Unislide" was driven by a Starret micrometer head with a 2.54 cm (1 inch) drive range accurate to $\pm$0.025 mm ($\pm$0.001 inch). The probe is shown schematically in Figure 15 and the entire assembly in Figure 16. In order to minimize local ice layer distortion in the vicinity of the probe, the flexible probe shaft was bent almost parallel to the ice layer surface and directed into the water flow as shown in Figure 15. In this configuration a greater length of the probe shaft was immersed in the thermal boundary layer at the ice-water interface and thus, the conduction of heat to the probe tip and subsequently to the ice surface was minimized. The ice surface was distorted a negligible amount if the probe was advanced toward the layer quickly and immediately withdrawn after a measurement was made. The prolonged presence of the probe at the interface did cause the layer to experience localized melting.

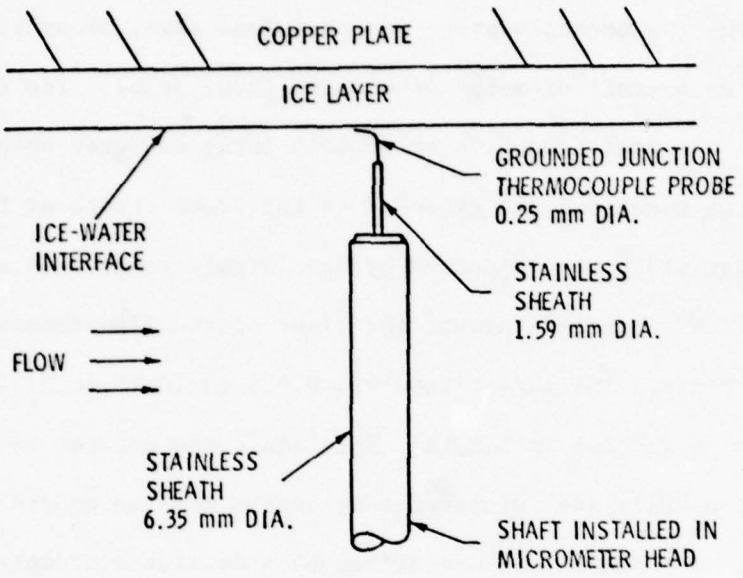

Figure 15. Mechanical-Thermocouple Probe

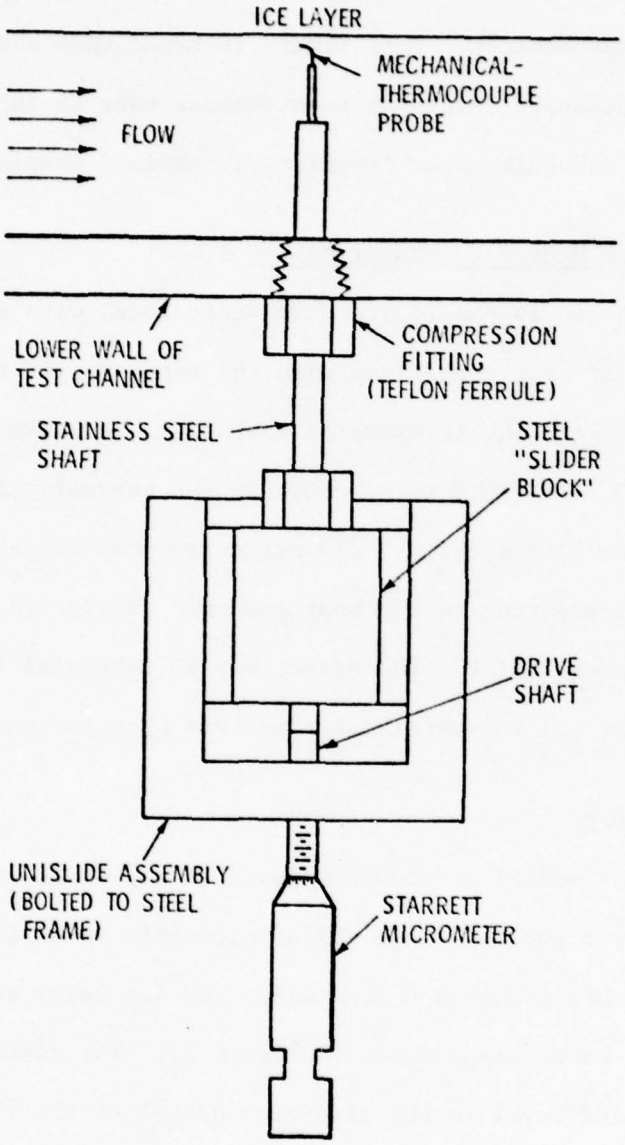

Figure 16. Ice Layer Thickness Measurement Apparatus

The uncertainty in ice layer thickness measurement by the technique described above was estimated to be no more than ± 0.05 mm for steady-state thickness measurements. This figure is based upon the variation encountered in successive thickness measurements made while the cooling plate temperature and bulk water temperature remained completely static.

D. Steady-State Heat Flux Measurements

In order to supply the finite difference model with accurate values of the parameter q^* for comparison with the experimental results, it was essential that q''_c, the interfacial heat flux, be known for a given flow condition and bulk fluid temperature in the channel. Because heat transfer conditions in the channel did not correspond to any simple solution presently existing in the heat transfer literature, it was decided that the most reliable and direct way to determine the convective film coefficient at the ice-water interface was by experiment.

1. Procedure

In the experimental procedure used, a steady-state ice layer was formed on the copper cooling plate while volumetric water flow rate and bulk temperature were maintained constant. The ice layer which formed was always of the basic shape shown in Figure 17. The surface of the layer was smooth and level in the direction normal to the flow indicating little or no cooling plate surface temperature variation in this direction. Even though care was taken to build up the ice layer slowly, some cracks would usually develop in the layer in a direction normal to the plane of the cooling plate surface. Because the cracks always formed in a direction parallel to the primary heat flow path, they were considered to have

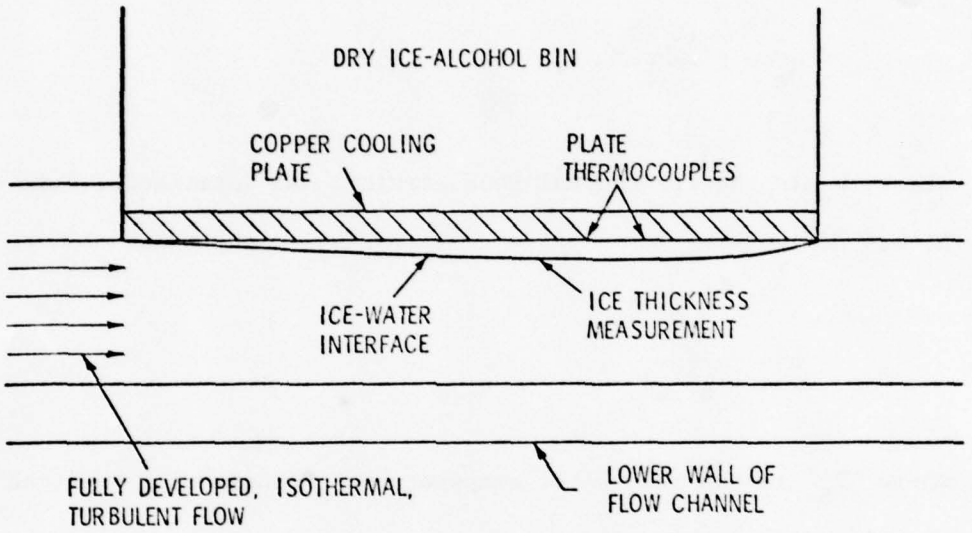

Figure 17. Sketch Illustrating the Basic Configuration of the Ice Layer on the Cooling Plate

a negligible effect on the heat conduction process in the layer. Otherwise, the ice was clear and homogeneous in appearance.

The steady-state ice layer thickness, S, was used to calculate q''_c, the interfacial heat flux, from the relation:

$$q''_c = k \frac{(T_m - T_w)}{S} \quad , \tag{34}$$

where k is the ice thermal conductivity. An interfacial film coefficient, h, was defined as

$$h = \frac{q''_c}{(T_b - T_m)} \quad , \tag{35}$$

where T_b is the bulk water temperature. Substituting Equation (35) in Equation (34) results in

$$h = (\frac{k}{S}) \frac{(T_m - T_w)}{(T_b - T_m)} \quad . \tag{36}$$

The plate temperature, T_w, in Equation (36) was determined from the outputs of the two plate thermocouples located immediately upstream and dowstream of the ice thickness measurement position. During each steady-state run, these two thermocouple outputs were recorded on a dual-channel strip chart recorder. T_w, in Equation (36), was given by the average of these two temperatures. Due to the rather close proximity of these thermocouples to the thickness measurement position and due to the very high thermal conductivity of the copper plate, this linear interpolation probably did not introduce significant error into the measurement of plate surface temperature. Also, from the two recorded plate temperatures, a

plate surface temperature gradient was calculated as an experimental check on the one-dimensional heat flow assumption. In all runs, the temperature gradient along the plate surface in the direction of flow was less than 1° C/cm and on the average was less than half this magnitude. The temperature gradients through the ice layer (normal to the plate surface), on the other hand, were always in the range 150-300° C/cm. From these results and the fact that the ice layer thickness was normally between 1 mm and 4 mm, it would seem reasonable to assume that heat conduction in the layer was very nearly one-dimensional. T_b, the fluid bulk temperature, was indicated by a thermocouple probe upstream of the test section. This temperature was also recorded on a strip chart recorder. Several ice thickness measurements were made during a single run by rapidly moving the probe tip toward the interface while observing the probe tip position through a magnifying lens. When the tip contacted the layer surface, the micrometer reading was noted and the probe quickly withdrawn so that deformation of the ice layer would not result. After a run was completed, the plate temperatures and the results of the thickness measurements were examined to ascertain which measurements were made while truly steady-state conditions prevailed. The steady-state condition was indicated by plate temperatures which changed negligibly with time and successive thickness measurements which showed essentially no solidification or melting of the layer. On the average, a single run would produce 3 to 5 thickness measurements taken in the presence of steady-state conditions. Only these data were used in the calculation of h .

The temperature difference $(T_m - T_w)$, an indication of the subcooling in the ice layer, ranged from -23°C to -58°C in the steady-state

experiments. Subcooling of this magnitude indicates that the thermal conductivity variation of the ice could be appreciable. Therefore, the conductivity, k, in Equation (36) was computed from the relation given by Ratcliff (20):

$$k\left(\frac{J}{cm\text{-}sec\text{-}^{\circ}C}\right) = \frac{7.8}{T(K)} - 0.00615 \quad . \tag{37}$$

This equation is valid for clear ice down to temperatures of -150°C. The value of k in Equation (36) was evaluated from Equation (37) at the temperature $(T_m - T_w)/2$ which represents an approximate mean temperature in the layer.

2. Uncertainty in the Prediction of Interface Film Coefficient

In performing the steady-state measurements, bulk fluid temperature and water flow rate were chosen so that the resultant steady-state ice thickness was not excessively small. Also, care was taken to keep the dry ice-methanol bath in a condition which would assure the lowest possible plate temperatures. These precautions were taken in order to minimize error in the measured value of h . From Equation (36), it is evident that small experimental errors in plate and bulk water temperature measurement and ice thickness measurement could cause significant error in the computed value of the film coefficient, h, if the magnitude of the errors in the temperature and thickness measurements are comparable to the quantities $(T_m - T_w)$, $(T_b - T_m)$, and S . The maximum possible error estimated for h, based upon the uncertainties in the measurements of S, T_w, and T_b (discussed in the previous section) did not exceed $\pm$7% for most of the steady-state runs. For a few runs at very high

interfacial heat flux where the ice layer was rather thin and the plate subcooling $(T_m - T_w)$ small, the maximum possible error in h was estimated to be as much as $\pm 10\%$. It should be emphasized that these estimated percentage errors in h represent upper bounds to the error and most probably the actual error in the prediction of film coefficient was much smaller.

E. Transient Ice Growth Measurements

The objective in the transient experiments was to compare experimental ice layer thickness measurements with the predictions of the finite difference model developed in Chapter II. It was therefore necessary to obtain T_w, q''_c, and S as functions of time in each transient run. Due to the nature of the mechanical probe technique for measuring transient ice layer thickness, only transients which involved growth of the ice layer were studied. Each run was classified as to the method by which the layer growth was initiated. There were basically two types of transient runs made; each is discussed in detail below.

1. Plate Temperature Transients

In this first type of transient, a steady-state ice layer was formed on the cooling plate by holding plate surface temperature, water flow rate, and bulk temperature constant. The plate surface temperature in this steady-state condition was maintained above -20°C by using a reduced amount of dry ice in the cooling bin. At time $t = 0$, ice layer growth was initiated by reducing the plate temperature while water flow rate and bulk water temperature and thus interface heat flux remained essentially constant.

The initial thickness, S_o, of the steady-state ice layer was not measured directly by the mechanical probe technique but instead was computed from the steady-state plate temperature and interfacial heat flux, the interface heat flux being determined from the bulk water temperature, the water flow rate, and the results of the steady-state heat flux experiments. This procedure was adopted for two reasons. First, the initial ice layer thickness, S_o, for the plate transient runs was rather small (less than 1 mm) so that a direct thickness measurement with the mechanical probe would introduce a $\pm$5% to $\pm$10% error into the S_o measurement (based upon $\pm$0.05 mm uncertainty in the thickness measurement). Also, due to the difficulties encountered in maintaining a steady plate temperature with a limited amount of dry ice in the coolant bin, it was very difficult to obtain an accurate measurement of S_o with the probe. Under these circumstances, prediction of the initial steady-state ice thickness S_o from the known quantities q''_c and T_w was considered to be the most reliable method.

Once steady-state had been achieved, a large quantity of dry ice was introduced into the coolant bin, rapidly lowering the plate surface temperature and initiating ice growth. The growth transient normally lasted approximately 4 to 6 minutes with the rate of growth rapidly decreasing with time. During the transient, the ice layer shape and appearance remained similar to that observed under steady-state conditions; i.e., the surface was smooth and level across the channel. The end of the transient was indicated by reestablishment of steady or quasi-steady conditions with respect to ice layer thickness and cooling plate temperature.

The variations of T_w and T_b with time were monitored by the strip chart recorder. T_b, the bulk water temperature, varied only slightly during a given run while the wall temperature, T_w, usually varied 30°C to 40°C. The ice layer thickness, S, was obtained by a mechanical probe technique somewhat modified from that used in the steady-state experiments. The probe tip was positioned approximately 0.3 mm to 0.6 mm below the steady-state ice layer surface at the start of a run. When the cooling plate temperature transient began, the ice layer grew and the layer surface approached the tip of the probe. When it was determined (by observation through the magnifying lens) that the layer had contacted the tip, the probe was quickly moved downward 0.127 mm (0.005 inch). This process was repeated as the layer grew and approached the probe at each new position. Simultaneously, the thermocouple output of the probe was recorded on a strip chart recorder. In this way, the chart trace indicated a sharp probe tip temperature rise each time the probe was pulled downward out of the thermal boundary layer. The trace of probe tip temperature represented a record of S, ice thickness, vs. time, in that the time elapsed between successive discontinuities in the strip chart trace indicated the time required for the layer to grow 0.127 mm. Normally, this procedure yielded from 10 to 20 thickness measurements in a single transient run, depending upon how much growth the layer experienced.

2. Combination Plate Temperature and Interface Heat Flux Transients

Runs of this type differed from the plate temperature transient runs in that the layer growth was induced by changes in both interface convective heat flux and cooling plate temperature. The procedure used

was to build a steady-state ice layer on the cooling plate with the coolant bin fully loaded with dry ice. The interface heat flux was maintained at a high level by maintaining high volumetric flow rates through the channel, so that the steady-state ice layer thickness would be small. In the combination plate temperature and interface heat flux transient runs, the initial ice thickness, S_o, was measured directly by the mechanical probe method. After this measurement had been made (time $t = 0$), the water flow rate was decreased to some intermediate value by rapidly closing the water throttling valve. This in turn decreased the interface heat flux and initiated ice layer growth. The change in heat flux occurred over such a short period of time (about 1 second) that, for all practical purposes, it was a step change. For times $t > 0$, the flow rate remained constant, as did the interface heat flux, except for a slight increase due to the small variation in bulk water temperature which occurred during the runs.

The step decrease in interface heat flux at time $t = 0$ always caused the cooling plate surface temperature to drop. High heat fluxes tended to drive the plate temperature higher while the plate temperature dropped under conditions of low interface heat flux. This behavior could be caused by a decrease in film coefficient in the coolant bin due to increased dry ice sublimation (and thus increased voidage) at the upper surface of the cooling plate under high interface heat flux conditions. Because of this dependence of plate surface temperature on interface heat flux, ice layer growth transients initiated only by a change in heat flux were not possible. Therefore, ice layer growth was due to a step decrease in interface heat flux at $t = 0$ followed by a slower drop in cooling plate surface temperature. Plate temperature and bulk water

temperature throughout these runs were recorded on strip chart recorders. Ice layer thickness measurements were obtained by the same method as that described for the plate transient runs. Table 5 (Chapter IV) summarizes the transient experiments.

3. Uncertainty in the Transient Measurements

The uncertainties involved in the measurements of water flow rate, bulk temperature, and plate temperature were stated in the description of these measurements. The estimated uncertainties also apply to the raw flow rate and temperature measurements obtained in the transient runs. However, the uncertainty in these raw measurements does not completely reflect the total uncertainty involved in the inputs to the finite difference model such as St and q* . The additional complications associated with the estimation of these parameters will be discussed later. The uncertainty in the raw measurement of S, the ice layer thickness, during the transient runs deviated from the estimated value of $\pm$0.05 mm stated in the section on ice thickness measurement. The $\pm$.05 mm applies primarily to the steady-state measurement of S . In the technique for measuring transient ice layer thickness, it was necessary that the probe remain near to the ice layer interface for an extended period of time (the probe tip was never more than 0.127 mm from the ice surface during most of the transient) and some local melting of the ice layer was observed in the immediate vicinity of the probe. Figure 18, a and b, shows schematically the type of layer deformation which occurred. In this figure, S' denotes the distorted layer thickness, while S is the thickness of the undisturbed layer under the same conditions. Thus, it is apparent that the thickness measurements made in the transient experiments indicate S' rather than the true, undisturbed thickness, S . A simple technique was therefore

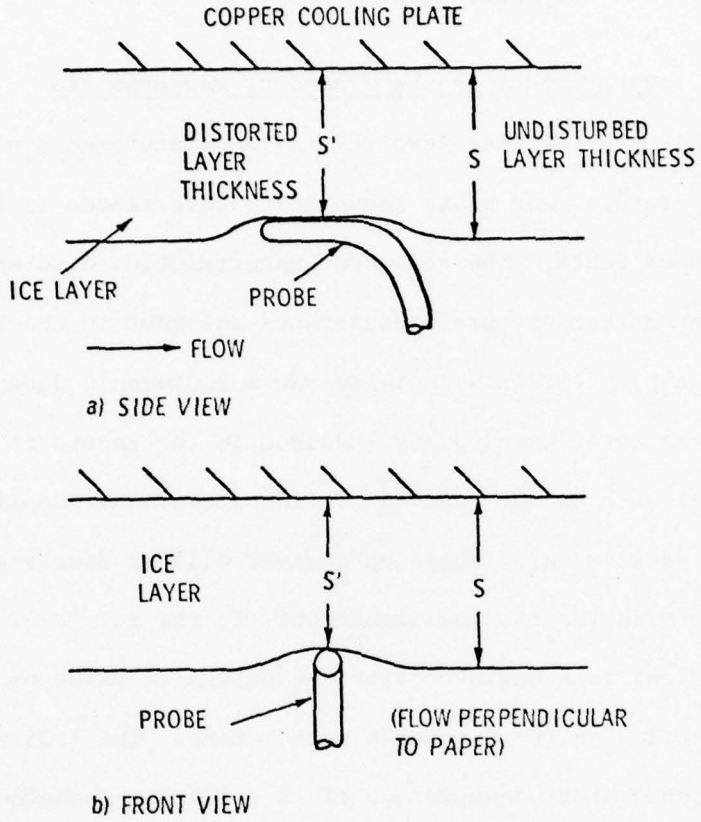

Figure 18. Sketch of Ice Layer Distortion During Transient Thickness Measurement

developed which would predict S, the true ice thickness, given the measured thickness S' and the flow conditions in the channel.

The phenomenon described above is thought to arise due to a distorted water flow pattern near the probe tip which in turn causes a local increase in the convective film coefficient at the interface. If this hypothesis is adopted, the interface film coefficient during transient ice thickness measurement becomes:

$$h' = h + \Delta h \quad , \tag{38}$$

in which h is the film coefficient for the given flow conditions over the undisturbed layer and Δh is the incremental increase in film coefficient due to the probe induced flow disturbance. During an ice layer growth transient, the conditions in the layer and at the ice layer surface are approximately as shown in Figure 19. An energy balance at the layer interface results in the following relationships.

For the undisturbed portion of the interface,

$$k \left.\frac{\partial T}{\partial y}\right|_{y=S} - q''_c = \rho \ell \frac{dS}{dt} \quad , \tag{39}$$

and for the disturbed interface immediately above the probe tip,

$$k \left.\frac{\partial T}{\partial y}\right|_{y=S'} - q'_c = \rho \ell \frac{dS'}{dt} \quad , \tag{40}$$

in which q'_c is the heat flux to the distorted portion of the layer surface; i.e.,

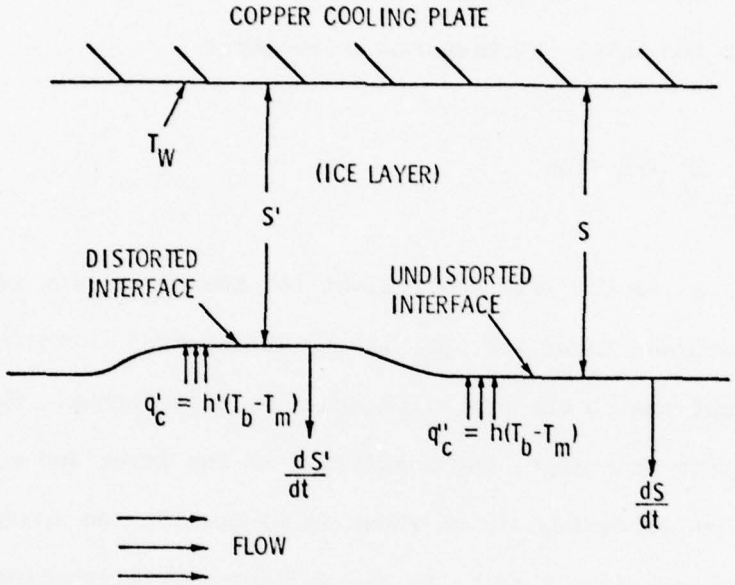

Figure 19. Distorted and Undistorted Interfaces During Ice Layer Growth Transient

$$q_c' = h'(T_b - T_m) = (h+\Delta h)(T_b - T_m) \quad . \tag{41}$$

In order to develop an approximate expression for S in terms of Δh and S', the following assumptions were made:

1. The temperature profile in the layer is approximately linear, thus;

$$\left.\frac{\partial T}{\partial y}\right|_{y=S} \simeq \frac{(T_m - T_w)}{S} \tag{42}$$

and

$$\left.\frac{\partial T}{\partial y}\right|_{y=S'} \simeq \frac{(T_m - T_w)}{S'} \quad . \tag{43}$$

This assumption is certainly satisfactory for the order of approximation sought here because of the small ratio of specific to latent heat $c/\ell \simeq 0.006°C^{-1}$.

2. The interface velocities $\frac{dS}{dt}$ and $\frac{dS'}{dt}$ are nearly equal:

$$\frac{dS}{dt} \simeq \frac{dS'}{dt} \quad , \tag{44}$$

which follows from the following reasoning. If the two interface velocities differed significantly in magnitude, the distortion of the interface would become more pronounced as the layer growth proceeded; this was not observed in the experiments.

Using these assumptions and combining Equations (34) and (40) yields:

$$k \frac{(T_m - T_w)}{S} - q_c'' = k \frac{(T_m - T_w)}{S'} - q_c' \quad . \tag{45}$$

By noting that,

$$q_c' = (h+\Delta h)(T_b - T_m) \tag{46}$$

and

$$q_c'' = h(T_b - T_m) \quad , \tag{47}$$

Equation (45) becomes:

$$\frac{S'}{S} = 1 - \left(\frac{S'\Delta h}{k}\right) \frac{(T_b - T_m)}{(T_m - T_w)} \quad . \tag{48}$$

Equation (48) relates S, the true, undisturbed ice layer thickness to the measured thickness S' and the incremental increase in film coefficient Δh . At a given time during a transient run, all quantities on the right-hand side of Equation (48), except Δh, are known. Δh was determined through a series of steady-state experiments. Under steady-state conditions,

$$h(T_b - T_m) = k \frac{(T_m - T_w)}{S} \qquad \text{(for the undisturbed interface)} \tag{49}$$

and

$$(h+\Delta h)(T_b - T_m) = k \frac{(T_m - T_w)}{S'} \qquad \text{(for the disturbed interface).} \tag{50}$$

Thus, for the steady-state ice layer,

$$\frac{h+\Delta h}{h} = \frac{S}{S'} \quad . \tag{51}$$

Both S and S' were determined by building a steady-state ice layer on the cooling plate. The probe was quickly advanced toward the layer surface and the thickness S of the undisturbed layer noted. The probe was allowed to remain in this position for 10 to 15 seconds during which time the layer receded slightly due to Δh, the local increase in film coefficient caused by the probe. Then, the probe was again moved upward until contacting the interface and S' was measured. Δh was then computed from Equation (51). Δh was found to be primarily a function of volumetric flow rate in the channel; therefore, measurements of Δh were made at the three volumetric flow rates used in the transient runs. The quantity $(h+\Delta h)/h$ is given in Table 2 for these three flow rates.

TABLE 2

Tabulation of the Quantity $(h+\Delta h)/h$

$Q(\frac{m^3}{sec})$	$\frac{h+\Delta h}{h}$
0.497×10^{-3}	1.008
0.639×10^{-3}	1.022
0.860×10^{-3}	1.038

CHAPTER IV

RESULTS AND DISCUSSION

A. Reduction of Experimental Data

The results of the steady-state heat flux measurements are used to obtain a correlation for interface film coefficient as a function of flow conditions within the test channel. Also, the analytic representation of the wall temperature variations obtained in the transient runs are discussed in some detail.

1. The Correlation for Interface Film Coefficient

The interfacial film coefficient, h, was assumed to be dependent upon only two flow variables, the volumetric rate of water flow through the test section and the bulk water temperature entering the test section. Curves were generated for the film coefficient as a function of bulk water temperature at constant flow rate for three different values of the flow rate Q, and bulk temperatures between 12°C and 24°C. A dimensional correlation of the form,

$$h = h[T_b] \quad , \qquad \text{(constant Q)} \qquad (52)$$

was found to be the most convenient for use in the transient experiments because the volumetric flow was always held constant in a given transient run. Dimensionless correlations of the form,

AD-A069 624 PENNSYLVANIA STATE UNIV UNIVERSITY PARK APPLIED RESE--ETC F/G 20/13
AN INVESTIGATION OF A TWO-PHASE, MOVING BOUNDARY SYSTEM, WITH C--ETC(U)
JAN 79 M W NANSTEEL N00024-79-C-6043
UNCLASSIFIED ARL/PSU/TM-79-32 NL

2 OF 2
AD A069624

END
DATE FILMED
7-79
DDC

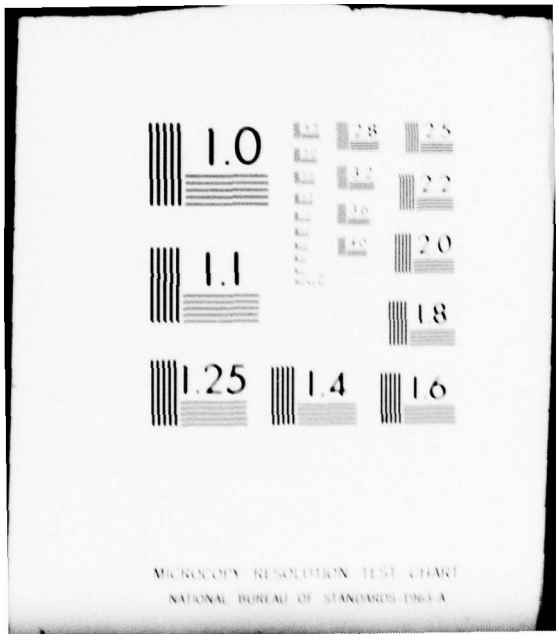
1.0
1.1
1.25
1.4
1.6
2.0
2.2
2.5
2.8
3.2
3.6
4.0
MICROCOPY RESOLUTION TEST CHART
NATIONAL BUREAU OF STANDARDS 1963-A

$$Nu = Nu[Re, \ Pr] \tag{53}$$

were found to be unsatisfactory because at constant flow rate, both Re and Pr vary with bulk temperature due to the sizeable viscosity variation of water in the range 12°C to 24°C. The three volumetric flow rates and the range of bulk water temperatures used in the correlation coincide with the flow rates and temperatures used in the transient runs.

The results of the steady-state heat flux experiments are shown in Figures 20, 21, and 22 for each of the three water flow rates. In these figures, the uncertainty associated with each of the discrete data points depends upon the cooling plate temperature, the bulk water temperature, and the steady-state ice layer thickness at the time of each heat flux measurement and, therefore, varies from data point to data point. The maximum value of the uncertainty in h occurring in the measurements at each flow rate is given in the figures.

The solid curves in Figures 20, 21, and 22 represent the results of the dimensionless correlation,

$$Nu = 0.0155 \ \sqrt{Pr} \ Re^{0.83} \ , \tag{54}$$

an equation given by Kays (19) for fully developed, turbulent flow in cylindrical tubes. In Equation (54), the hydraulic diameter of the flow channel was used in forming the dimensionless parameters Nu and Re . This correlation gives a rough estimate of the film coefficient at the ice-water interface, useful for comparison with the results of the experimental correlation.

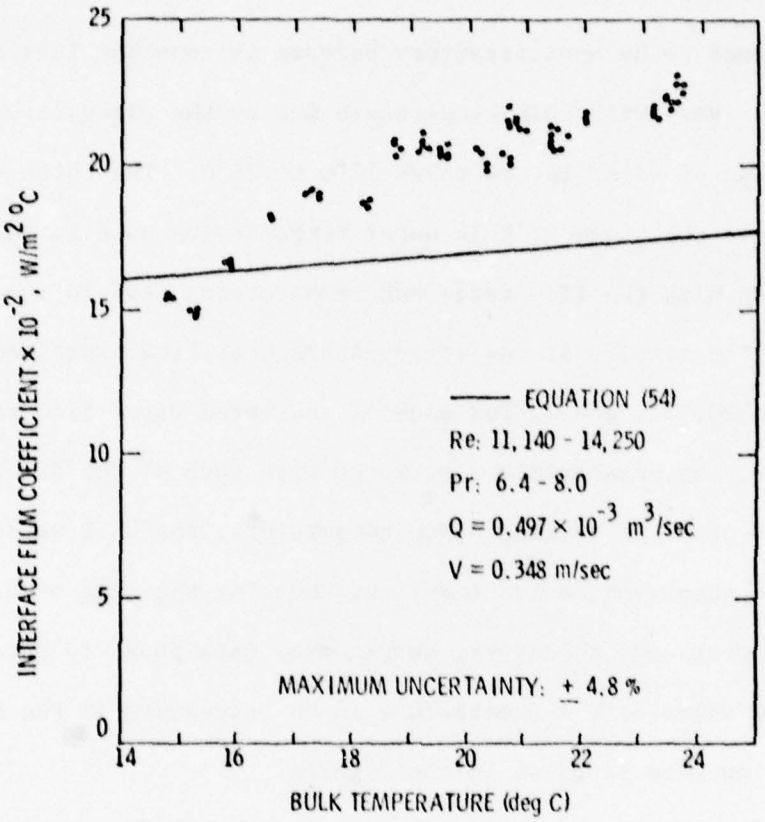

Figure 20. Interface Film Coefficient Versus Bulk Water Temperature, Q = 0.497 X 10^{-3} m^3/sec

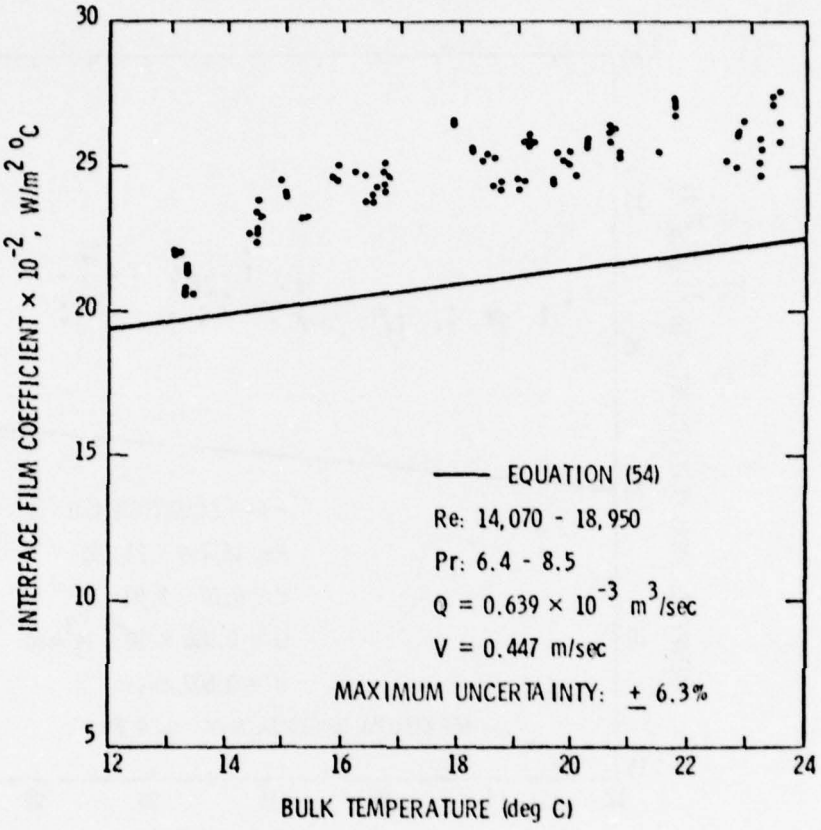

Figure 21. Interface Film Coefficient Versus Bulk Water Temperature, Q = 0.639 X 10^{-3} m^3/sec

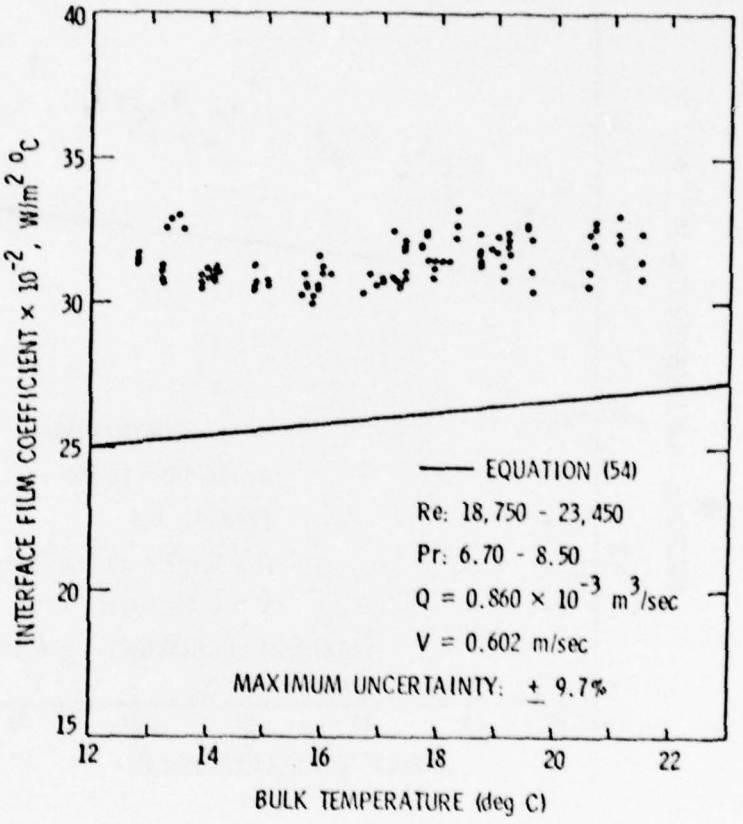

Figure 22. Interface Film Coefficient Versus Bulk Water Temperature, Q = 0.860 X 10^{-3} m^3/sec

The results shown in Figures 20 through 22 indicate that for each flow rate, the flow at the ice thickness measurement position is not fully developed thermally. This is not unexpected because cooling takes place for a length of only 3.5 hydraulic diameters before the point of heat flux measurement. Also, it should be pointed out that the commonly used dimensionless fluid property and flow parameters Pr and Re behave approximately as

$$RePr = CONSTANT \tag{55}$$

in each of Figures 20, 21, and 22. Therefore, when moving to the left on the abscissa (decreasing T_b), Pr is increasing while Re is decreasing according to Equation (55). The experimental value of h decreases with decreasing bulk temperature for basically two reasons. First, Re in the channel is decreasing as bulk temperature is lowered. This should cause the film coefficient to decrease even though Pr is increasing, because Nu is generally a stronger function of Re than Pr . Secondly, because Pr is increasing with decreased bulk temperature, the temperature profile should be more nearly fully developed at lower temperature, resulting in decreased film coefficients. The effect of increased Pr on the rate of thermal development in turbulent channel flow is demonstrated by Kays (19). The downward slope of the data for increased Pr (decreasing T_b) is seen to be less and less apparent as flow rate is increased; in fact, in Figure 22, the effect is nearly undetectable. This indicates that the effects of Pr on the flow development may become less pronounced at higher Re (higher flow rate).

For the purpose of comparison, the data of Figures 20, 21, and 22 are replotted in Figure 23. In this figure, the solid lines represent least square (polynomial) curve fits to the three data sets. The absolute spread in the data is seen to be largest for the top (high flow rate) curve in Figure 23. This reflects the difficulties in maintaining sufficiently low cooling plate temperatures and adequate ice layer thickness in the presence of the high interfacial heat fluxes. Table 3 provides a brief summary of the results of the steady-state heat flux measurements. In this table, "V" is the average flow velocity in the flow channel just upstream of the cooling plate leading edge, $(DEV)_{rms}$ is the root mean square deviation of the data from the curve generated by least squares, and $(DEV)_{max}$ is the maximum percentage deviation from the least squares curve.

The results tabulated in Table 3 show that the prediction of interfacial film coefficient is probably not in error by more than $\pm 5\%$.

2. Cooling Plate Temperature Variations

During the ten transient ice growth experiments, cooling plate surface temperatures were measured as a function of time. It was necessary that these temperature variations be placed in a form, $T_w(t)$, which would permit reliable, accurate wall temperatures (and derivatives) to be computed for any given time, t.

Due to the rapid plate surface temperature drop during the first few moments of the transient runs and the asymptotic approach toward a steady-state plate temperature, polynomial curve fits by the method of least squares of the form

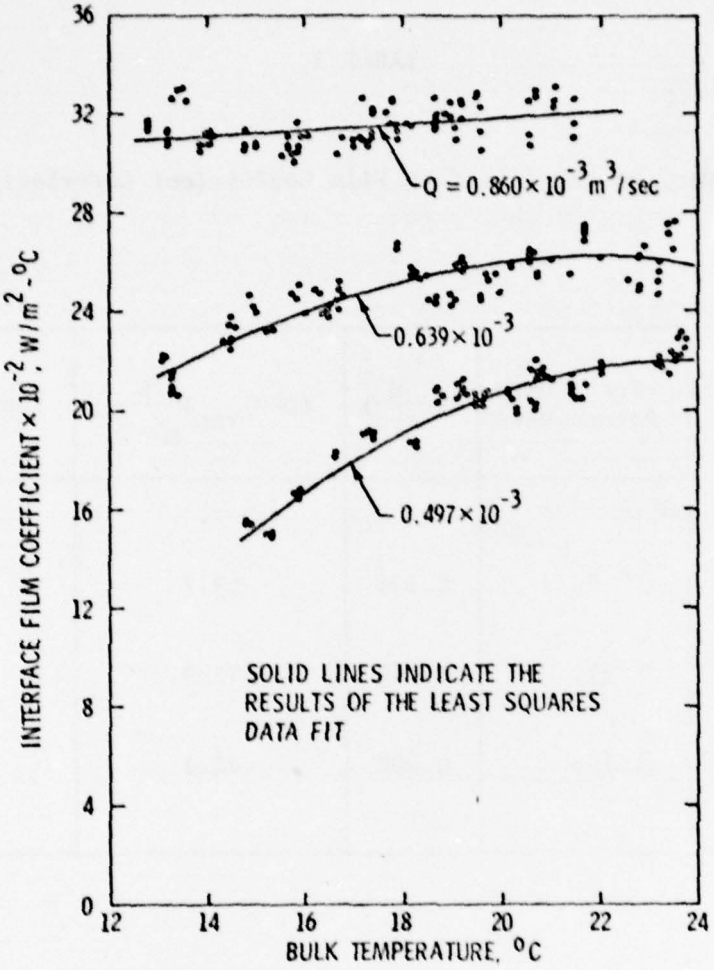

Figure 23. Results of the Interface Film Coefficient Correlation

TABLE 3

Summary of the Interface Film Coefficient Correlation

$Q(\frac{m^3}{sec})$	Total Data Points Used	$V(\frac{m}{sec})$	$(DEV)_{rms}(\frac{W}{m^2 \cdot °C})$	$(DEV)_{max}(\%)$
0.497×10^{-3}	96	0.348	59.2	5.7
0.639×10^{-3}	111	0.447	72.9	6.2
0.860×10^{-3}	108	0.602	72.1	6.4

$$T_w = \sum_{m=0}^{M} a_m t^m \qquad \text{(M = Degree of Polynomial)} \qquad (56)$$

did not satisfactorily represent the experimental data. Therefore, the plate temperature data was represented by rational functions of the form

$$T_w = \frac{A_1+A_2t+A_3t^2 \ldots +A_{J+1}t^J}{1+B_1t+B_2t^2 \ldots +B_Kt^K} = \frac{\sum_{j=0}^{J} A_{j+1}t^j}{1+\sum_{k=1}^{K} B_kt^k} \quad , \qquad (57)$$

where the A_j and B_k are constants and J and K each ranged between 1 and 7.

This form of equation allows much more flexibility than Equation (56) in the type of functional relationship which is to be represented. This is because a simple polynomial expression such as Equation (56) cannot have any poles and thus, cannot easily approximate functions with singularities. Equation (57), on the other hand, may have as many as K distinct poles. This characteristic makes the rational function ideal for the representation of many critical phenomena [see Baker (21)], and functions which are singular or nearly singular. However, a problem arises in that the poles of Equation (57) may occur anywhere within the domain of the original function, and these singularities may be undesirable.

The constants A_j and B_k were chosen so that Equation (57) would collocate or coincide with the experimental data points at $J + K + 1$ points, spaced evenly with respect to the temperature measurements. For a given transient run, these coefficients were computed for all permutations and combinations of J and K from $J = 1$, $K = 1$, to $J = 7$, $K = 7$ resulting in 49 different rational function correlations for T_w.

From this group, one was chosen which resulted in the best fit of the data and which had no poles within the time domain of interest. Figure 24 shows the fit obtained for transient run 5, in which the rational function used had a numerator of degree 1 and a denominator of degree 4. The fit is seen to be good for all values of t including small t where plate temperature is dropping rapidly.

The derivative $\frac{dSt}{dt^*}$ requires the evaluation of $\frac{dT_w}{dt^*}$ from the transient experimental data, this term was evaluated through differentation of Equation (57):

$$\frac{dT_w}{dt} = \frac{\sum_{j=0}^{J} j\, A_{j+1} t^{j-1}}{1 + \sum_{k=1}^{K} B_k t^k} - \frac{\left(\sum_{k=1}^{K} kB_k t^{k-1}\right)\left(\sum_{j=0}^{J} A_{j+1} t^j\right)}{\left(1 + \sum_{k=1}^{K} B_k t^k\right)^2} . \qquad (58)$$

The results of the rational function approximations for all ten transient runs are shown in Table 4. In this table,

$$\text{RMS ERROR} = \left[\frac{\sum_{i=1}^{I} [T_{wi} - R(t_i)]^2}{I}\right]^{1/2} \qquad (59)$$

in which T_{wi} is the measured wall temperature at $t = t_i$, $R(t_i)$ is the rational function approximation to T_{wi}, and I is the number of data points used in the correlation.

B. Analytical Results

1. Results of the Finite Difference Model

Sample results of the finite difference calculation for the solid layer thickness were generated for four cases. It was assumed in all cases that the solid layer is in a state of equilibrium prior to the time $t = 0$. The initial temperature profile in the layer then, is

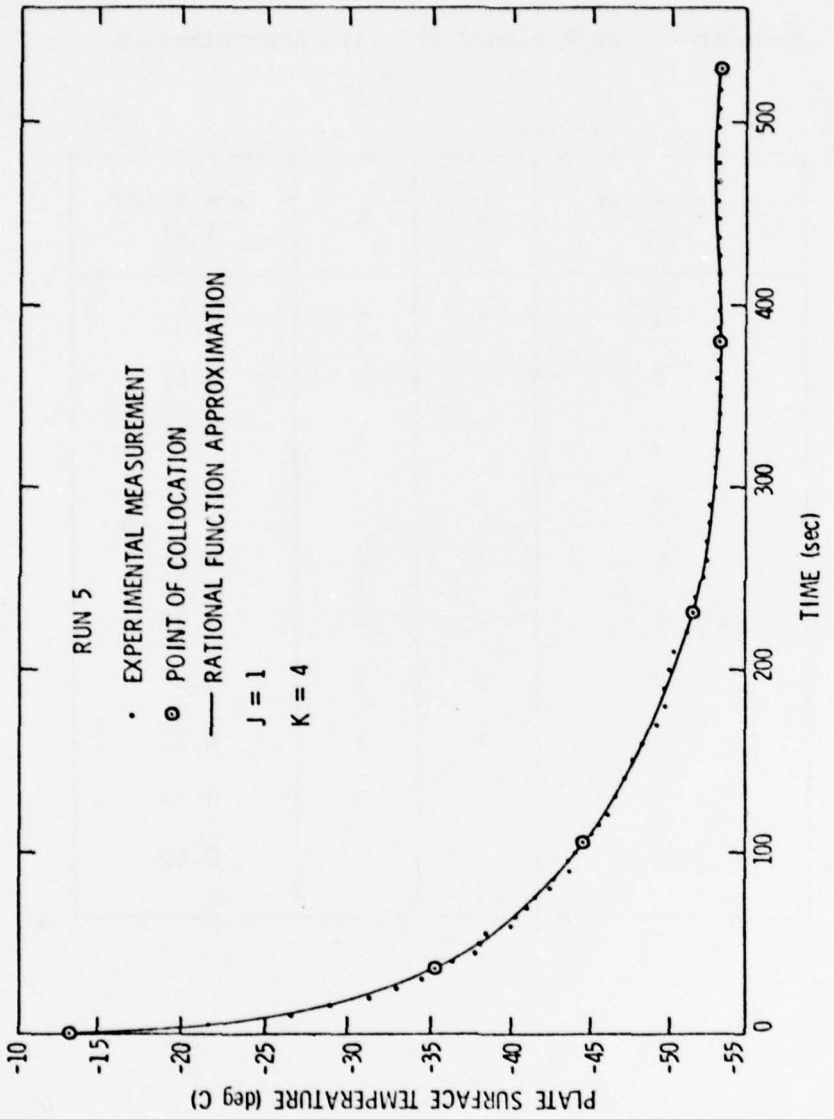

Figure 24. The Rational Function Curve Fit for T_w, Transient Run 5

TABLE 4

Results of the Rational Function Approximations

Transient Run	J	K	RMS ERROR (°C)
1	1	3	0.51
2	1	4	0.62
3	6	1	0.54
4	5	2	0.28
5	1	4	0.48
6	1	4	0.28
7	2	7	0.14
8	1	5	0.22
9	1	3	0.24
10	3	1	0.40

given by:

$$\theta_o(y^*) = y^* \qquad (t^* = 0) \quad , \tag{60}$$

i.e., the initial temperature profile is linear. This assumption, however, need not be made as the model may allow initial conditions other than steady-state. At time $t^* = 0$, either the wall temperature or the interface heat flux changes in a stepwise manner, thus, initiating solid layer solidification or melting. The initial values of St and q^* (before layer growth or decay begins, i.e., for $t^* < 0$) are indicated by the subscript "i", while the unsubscripted symbols refer to the values of the parameters for times $t^* \geq 0$. Note that for a steady-state layer initially,

$$St_i = q_i^* \tag{61}$$

and that the final steady-state value of S^* is given by,

$$S^* = \frac{St}{q^*} \qquad \text{(at steady-state)} \quad . \tag{62}$$

In Figures 25 and 26, the behavior of the solid layer is shown in terms of the dimensionless coordinates S^* and t^*. In these figures the interface heat flux is held constant while the wall temperature is decreased promoting solid layer growth; while in Figure 26, the wall temperature is increased causing the layer to melt. Both figures clearly show the significant effect which the parameter St has on the layer transient behavior. In Figure 25 (solidification), the interface velocity

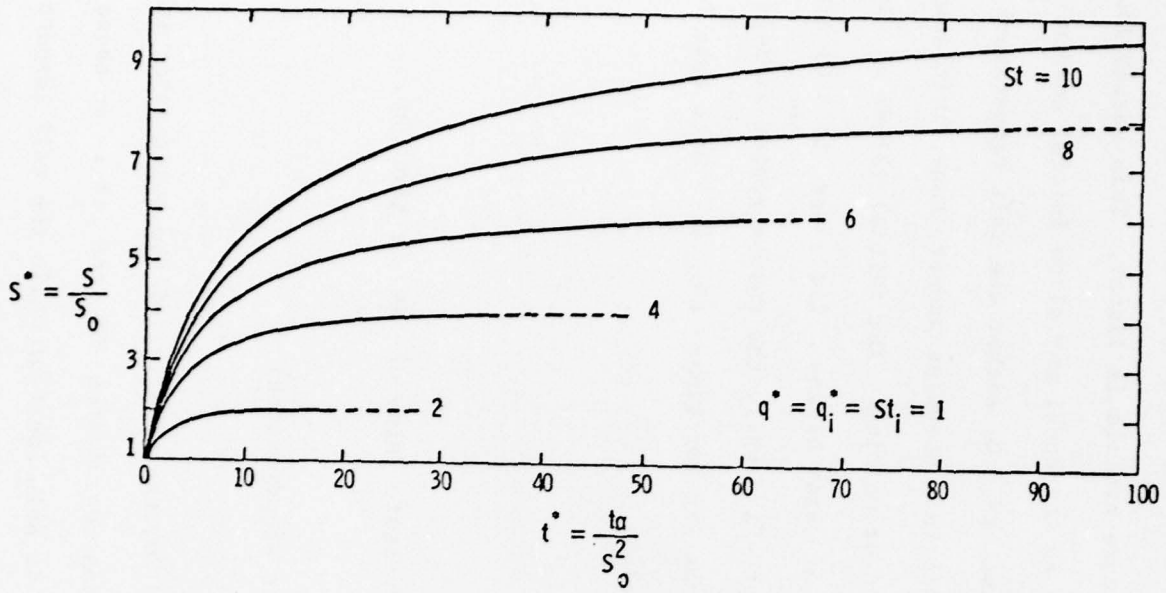

Figure 25. S* Versus t*, Constant Heat Flux, Wall Temperature Stepped Down

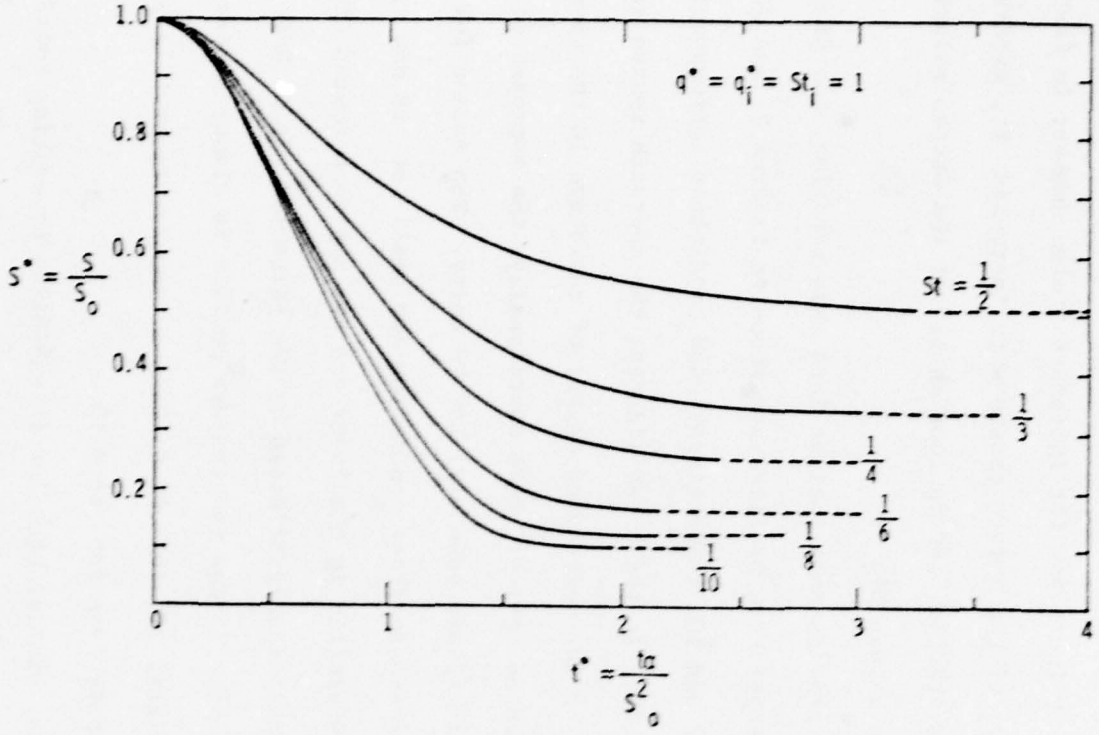

Figure 26. S* Versus t*, Constant Heat Flux, Wall Temperature Stepped Up

dS^*/dt^* is initially zero; the initial velocity appears to be non-zero only because the time scale in Figure 25 is too coarse for the initial period of rapid acceleration to be clearly seen. The most important aspect of the curves in Figure 25 is the effect of St on the time required for the layer to assume a new steady-state thickness. This time is substantially increased for increased Stefan number; in fact, even the basic shape of the curves change with increased St, eventually assuming the characteristic "square root shape" of the Stefan solution, (2), for very large values of St .

In order to provide some insight into this behavior, the dimensionless solid layer temperature profiles are shown in Figures 27 and 28 for Stefan numbers of 2 and 10, respectively, and conditions corresponding to those in Figure 25. In these two figures, the approach toward steady-state is indicated by the decreasing degree of curvature in the temperature profiles (for increased t^*) or, more specifically, the approach of the slope at $y^*/S^* = 1$ (phase boundary) toward unity. The reason for the rapid attainment of steady-state conditions for small St is now clear, for the temperature profile in the layer and its approach toward the steady-state is significantly affected by the parameter St . Note that in Figure 27, for $St = 2$, the temperature profile is almost linear at $t^* = 1$, while in Figure 28, for $St = 10$, the temperature profile possesses considerable curvature even for $t^* = 10$.

In Figure 26, similar behavior is exhibited by melting solid layers. The initial interface velocity is again zero and the melting rate is seen to increase with decreased St . For very small St, the dimensionless layer thickness, S^*, becomes approximately a linear function of t^* as is apparent from the interface energy balance condition (5f); i.e.,

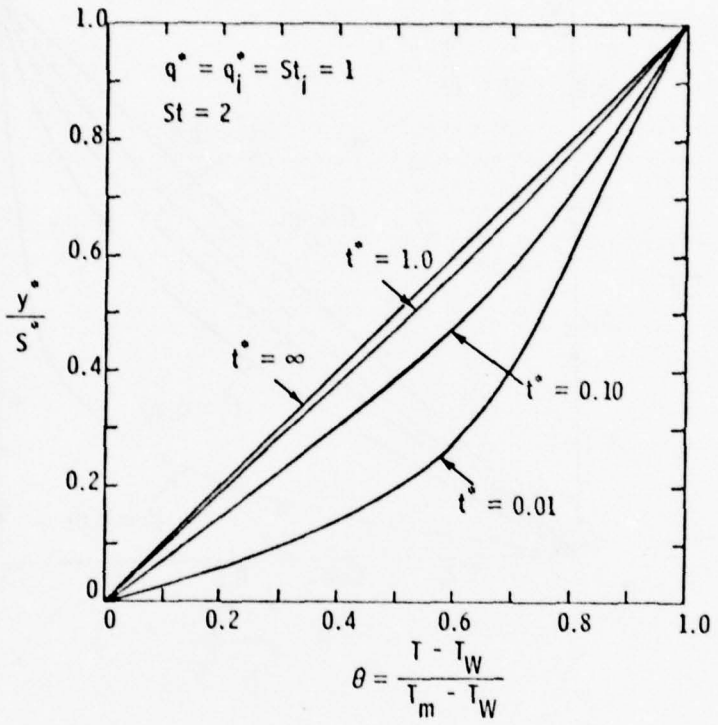

Figure 27. Dimensionless Solid Layer Temperature Profiles, St = 2

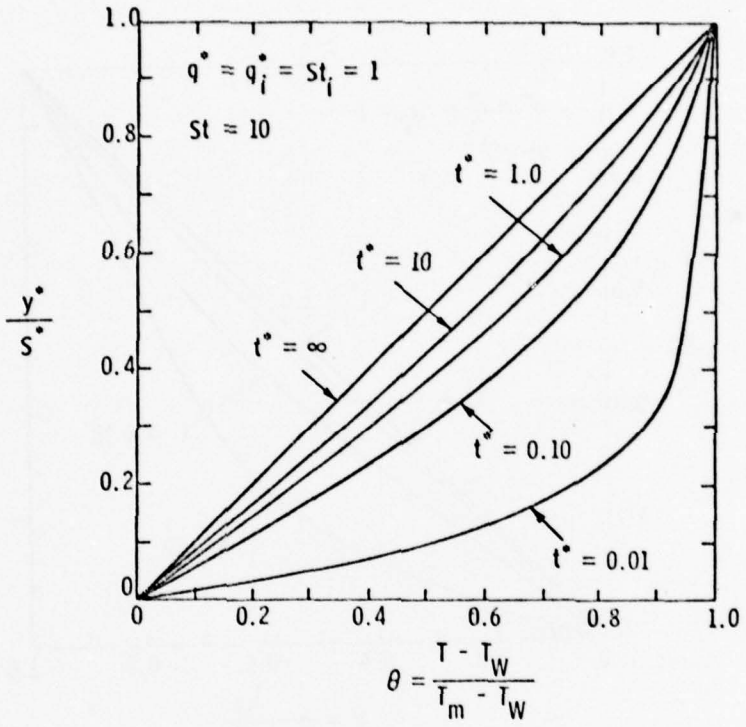

Figure 28. Dimensionless Solid Layer Temperature Profiles, St = 10

$$\left.\begin{aligned} \frac{dS^*}{dt^*} &\simeq -q^* \qquad (63) \\ S^* &\simeq 1-q^*t^* \qquad (64) \end{aligned}\right\} \quad St \to 0 \ .$$

It should also be noted that Equation (64) is the limit of Equation (10), the asymptotic solution, as $St \to 0$. As in Figure 25, the time required for the layer thickness to reach a new steady-state value is again largely dependent upon St . Steady-state is seen to be attained more quickly for small St than for large St, even though more of the layer must melt when St is small.

In Figures 29 and 30, the solid layer behavior is shown for the constant wall temperature case where interface heat flux is decreased (Figure 29) and increased (Figure 30) resulting in solidifying and melting solid layers, respectively. In Figure 29, the interface velocity is non-zero at $t^* = 0$. The layer growth profiles in Figure 29 are similar in shape to those in Figure 25 for constant heat flux; however, in this case, it is the interfacial heat flux parameter, q^*, which governs the rate at which steady-state conditions are attained. In Figure 30, the heat flux is increased at $t^* = 0$ so that the solid layer melts down to some fraction of its original thickness. Once again, very large values of the heat flux cause the layer to melt at a rate which is almost constant, and reach a new steady-state very quickly. The one obvious conclusion which may be drawn from Figures 25, 26, 29 and 30 is that both St and q^* not only govern the magnitude of the final steady-state layer thickness, but more impertantly, these parameters govern the character of the solution $S^*(t^*)$ and the duration of the transient.

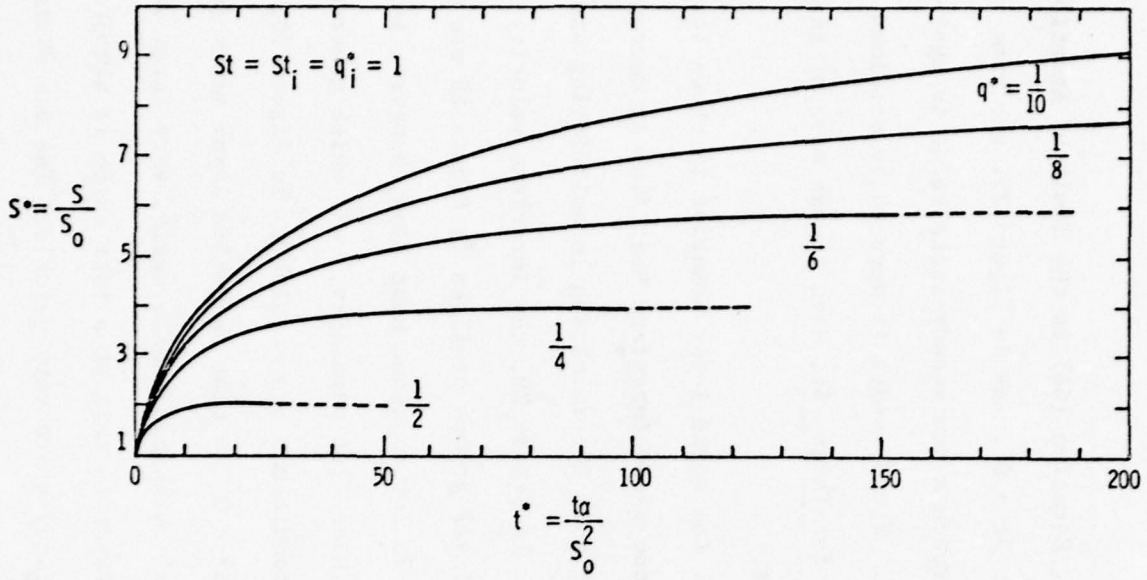

Figure 29. S* Versus t*, Constant Wall Temperature, Heat Flux Stepped Down.

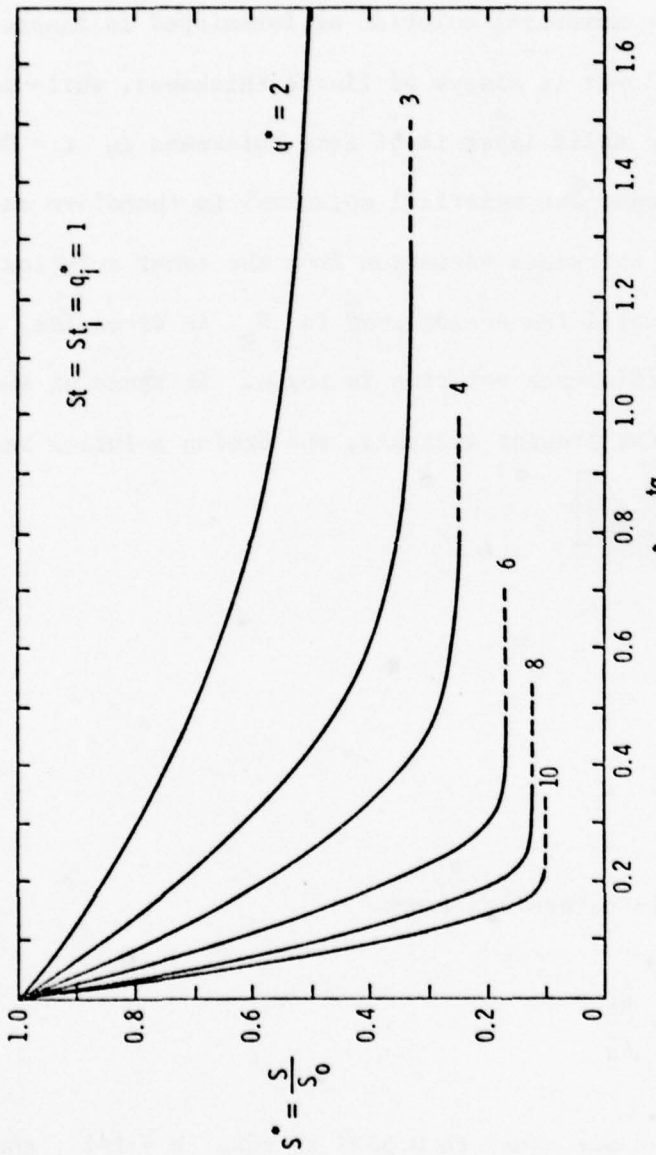

Figure 30. S* Versus t*, Constant Wall Temperature, Heat Flux Stepped Up

In order to illustrate the accuracy and effectiveness of the finite difference model, at least for a simple case of constant wall temperature solidification, the numerical solution is compared with the exact solution of Stefan (2). An inconsistency arises in this comparison due to the fact that the numerical solution as formulated in Chapter II assumes that the solid layer is always of finite thickness, while in the Stefan solution, the solid layer is of zero thickness as $t = 0$. The comparison of the exact and numerical solutions is therefore made by initially computing the thickness variation from the exact solution and continuing in this way until the solid layer is S_o in dimension, at which time the finite difference solution is begun. In terms of the pertinent variables of the present analysis, the Stefan solution becomes:

$$\theta = \frac{\operatorname{erf}\left[\dfrac{y^*}{2\sqrt{t^*+1/4b^2}}\right]}{\operatorname{erf}(b)} \quad , \tag{65}$$

and

$$S^* = 4b^2 t^* + 1 \quad , \tag{66}$$

where the constant b is determined from:

$$b^2 e^{b^2} \operatorname{erf}(b) = \frac{St}{\sqrt{\pi}} \quad . \tag{67}$$

For convenience, St was set equal to 0.5923 so that $b = 1/2$; then, Equation (66) becomes:

$$S^* = \sqrt{t^*+1} \quad . \tag{68}$$

The results of Equation (68) and the finite difference solution are compared in Figure 31. This figure indicates that, at least in this simple case, there is essentially no difference between the exact and numerical solutions. The results of this comparison and the results of others to follow indicate that the finite difference solution technique does indeed converge to the exact solution of the system, Equations (5).

2. Evaluation of the Approximate Solution Techniques

It was mentioned previously that the extent to which the approximate techniques of solution (asymptotic and integral) are capable of representing the exact solution can only be established through quantitative comparison with methods which are believed to be exact. Below, the overall effectiveness of each of the approximate techniques is investigated.

In Figure 32, the asymptotic solution for small St is compared with the finite difference numerical solution for Stefan numbers of 1/50, 1/10, and 1. From this figure, the effect of St on the accuracy of the asymptotic solution is evident. For St as large as 1/10, the approximate solution represents the true solution with little error, while for St = 1, the accuracy of the asymptotic solution rapidly decays. The capability of the asymptotic solution in yielding accurate results depends primarily upon how well the assumed, linear solid layer temperature profile approximates the actual temperature profile. The actual temperature profiles (computed from the full finite difference numerical solution) are shown in Figure 33 for the conditions of Figure 32 and Stefan numbers of 1 and 1/50. The curves in this figure clearly indicate that for any time, t^*, the profile for small St is a substantially better approximation to the steady-state, linear profile than the profile for

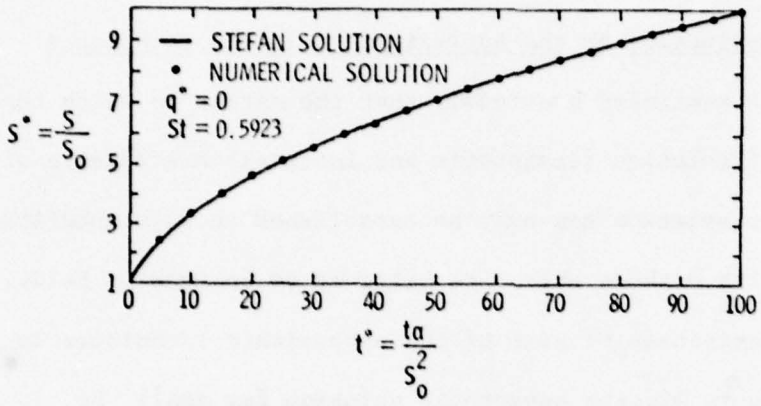

Figure 31. Comparison of Exact (Stefan) and Numerical Solutions

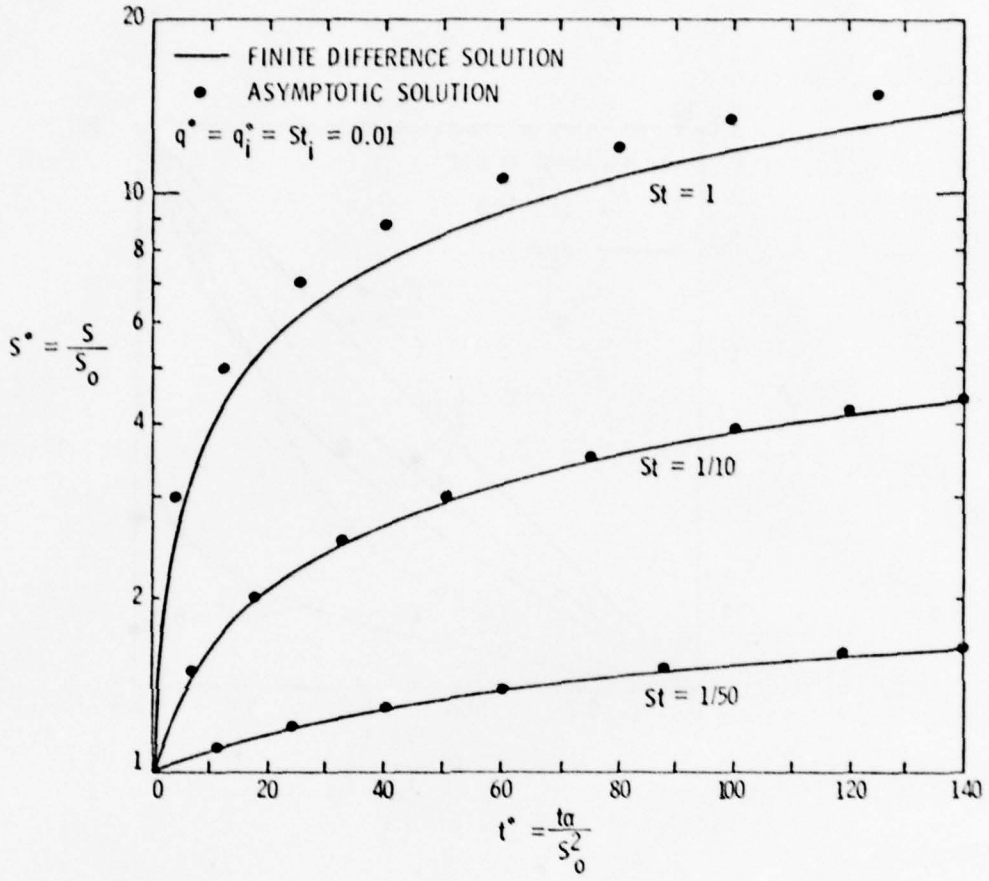

Figure 32. Asymptotic Behavior for Small St

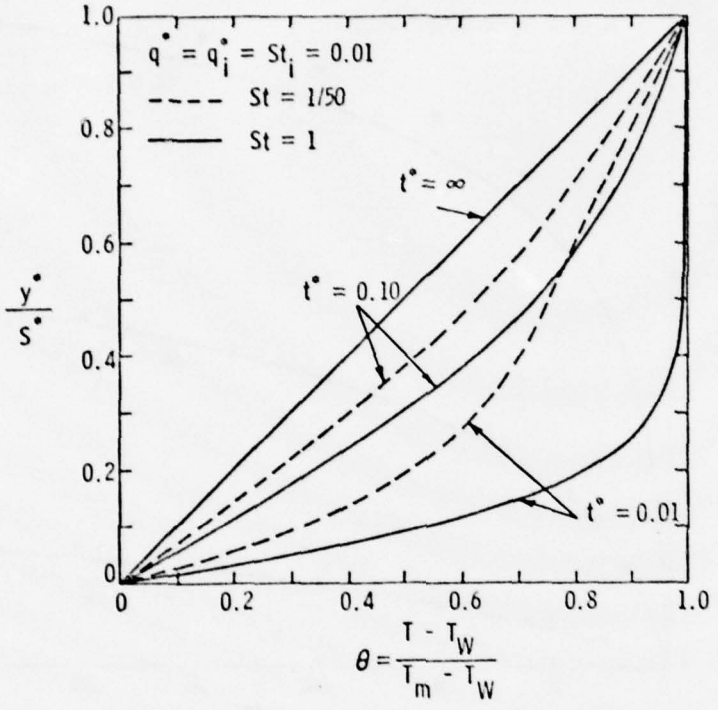

Figure 33. Dimensionless Solid Layer Temperature Profiles, St = 1/50 and 1

large St and it therefore follows that the asymptotic solution yields more accurate results when St is small. The conclusion drawn from the above discussion is that the asymptotic solution, Equation (10), does yield an accurate, simple means of estimating the solid layer thickness variation for small values of the parameter St . Of course, for instances in which St and/or q* are not constant, Equation (9) must be used in computing S* rather than Equation (10). The practical utility of Equations (9) and (10) depend primarily upon the specific substance and wall temperature variation in the problem under consideration i.e. the magnitude of $St = c(T_m - T_w)/\ell$. Ice $(\ell/c \simeq 160°C)$ is one substance for which the asymptotic solution could prove very useful provided that the subcooling $(T_m - T_w)$ in the ice layer is small compared with ℓ/c ; this is often a good assumption.

In Figures 34 through 36, the approximate integral solution, Equation (19), is shown plotted along with the exact numerical solution for Stefan numbers 2, 5, and 10. Unlike the asymptotic solution, the integral solution tends to yield reasonably accurate solid layer thickness results independent of St . In all of the plots the maximum error in the integral solution tends to be about 5%, the larger errors occurring for small time t* . Evidently, the parabolic temperature profile assumed in Equation (18) does reasonably well in approximating the actual solid layer temperature profile and does especially well for large time, t*, when the profile tends toward the linear, steady-state shape. From these results it appears that the integral solution technique may be as general a solution method and nearly as accurate as the finite difference solution and this is indeed true for many situations. However, the form of Equation (19) is such that dSt/dt* and dq*/dt*

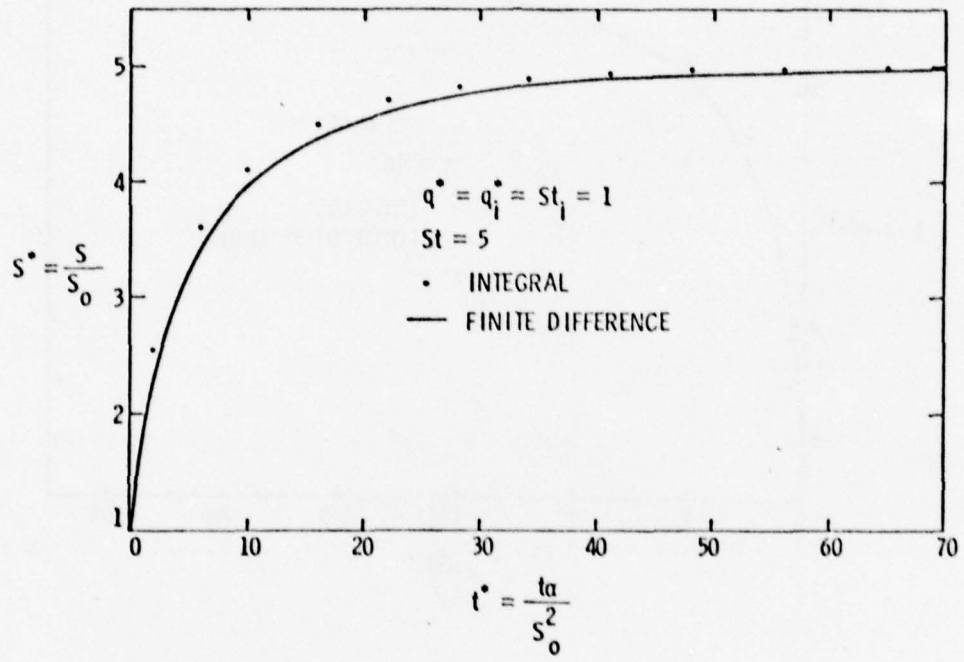

Figure 35. Comparison of Integral and Finite Difference Solutions, St = 5

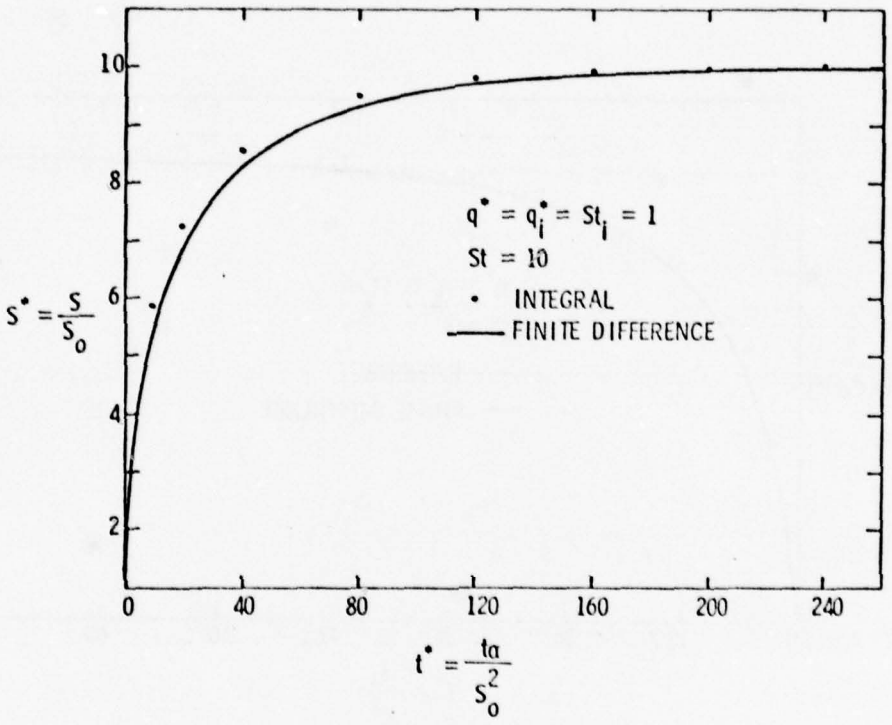

Figure 36. Comparison of Integral and Finite Difference Solutions, St = 10

are required for the integral solution of problems in which St and q* are both time dependent. This factor can make the integral technique somewhat inconvenient when neither wall temperature nor interface heat flux are known precisely as functions of time; in such situations the finite difference solution is the more appropriate.

C. Evaluation of the Mathematical Model

In the previous sections the basic methods of solution (asymptotic, integral, and finite difference) were tested and evaluated with respect to their ability to generate accurate solutions to the general mathematical model as formulated in Chapter II. In this section, the model itself and the assumptions and simplifications made in its development are tested and evaluated via the results of the transient ice growth measurements described in Chapter III.

The results of the ten transient tests are compared with the predictions of the finite difference computer model in Figures 37 through 46, while Table 5 indicates the type of transient and the conditions present in the flow channel for each of the ten runs. The computer predictions are indicated by the solid curves while the results of the transient ice thickness measurements are represented by the data points. The range of uncertainty shown with each data point corresponds to the ± 0.05 mm uncertainty in the transient ice thickness measurement after the correction was made for ice layer distortion. In Figures 31 through 41 (plate transient runs), the agreement between the experimental and computer results (the computer predictions are indicated by the solid curves) is seen to be good for all values of the dimensionless time t^*. There is some tendency for the model to overpredict the ice layer growth

TABLE 5

Summary of Conditions for Transient Runs

Run	Type of Transient	Flow Rate $X_3 1000$ (m^3/sec)	Bulk Temp. (°C)	$Re = VD_h/\nu$
1	PLATE	0.639	17.6	15,830
2	PLATE	0.639	19.0	16,390
3	PLATE	0.639	18.3	16,110
4	PLATE	0.860	15.7	20,300
5	PLATE	0.497	20.7	13,270
6	COMB.	0.639	19.2	16,480
7	COMB.	0.639	15.5	15,000
8	COMB.	0.497	18.2	12,490
9	COMB.	0.639	17.8	15,910
10	COMB.	0.860	15.8	20,350

Note: "PLATE" denotes plate temperature transient.

"COMB." denotes combination plate temperature and interface heat flux transient.

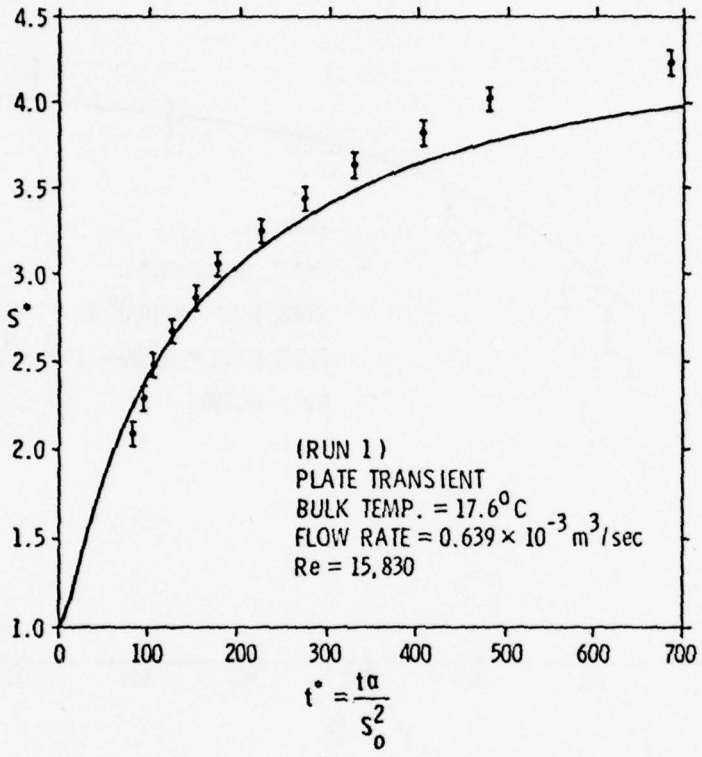

Figure 37. Results of Transient Run 1

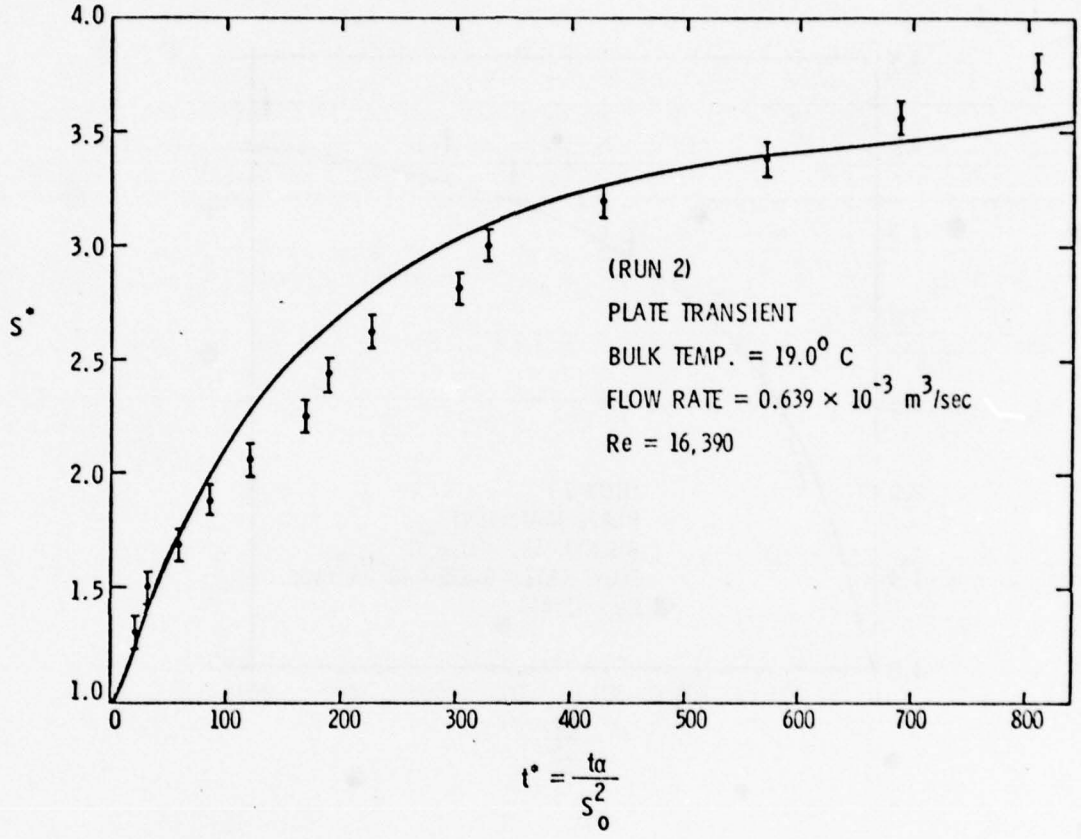

Figure 38. Results of Transient Run 2

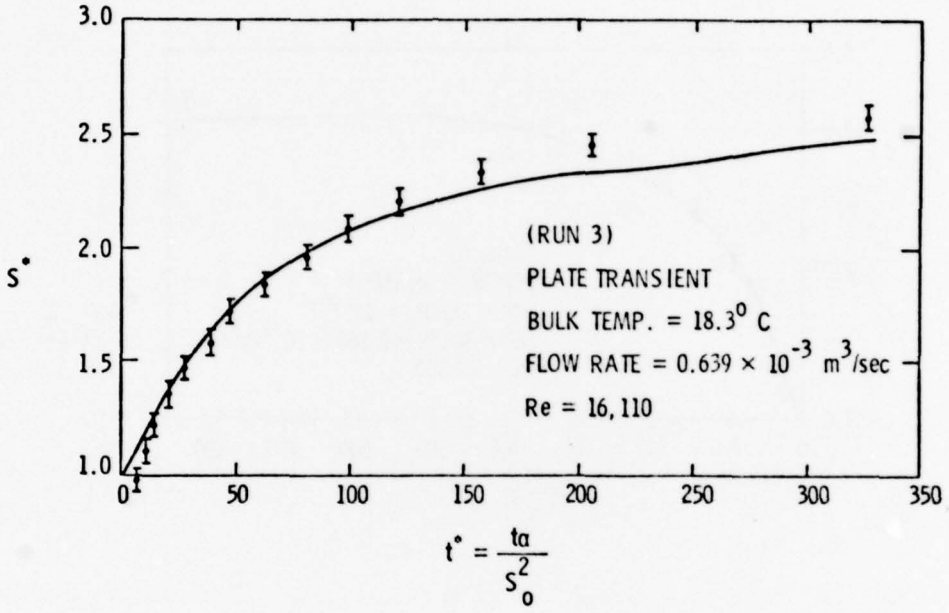

Figure 39. Results of Transient Run 3

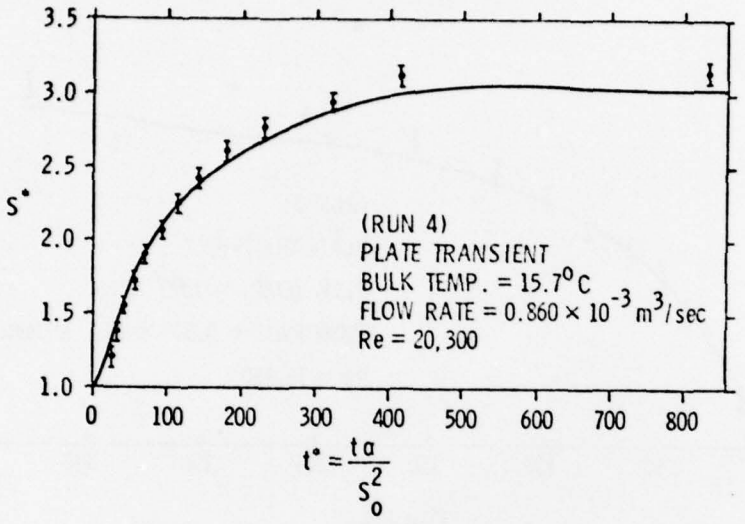

Figure 40. Results of Transient Run 4

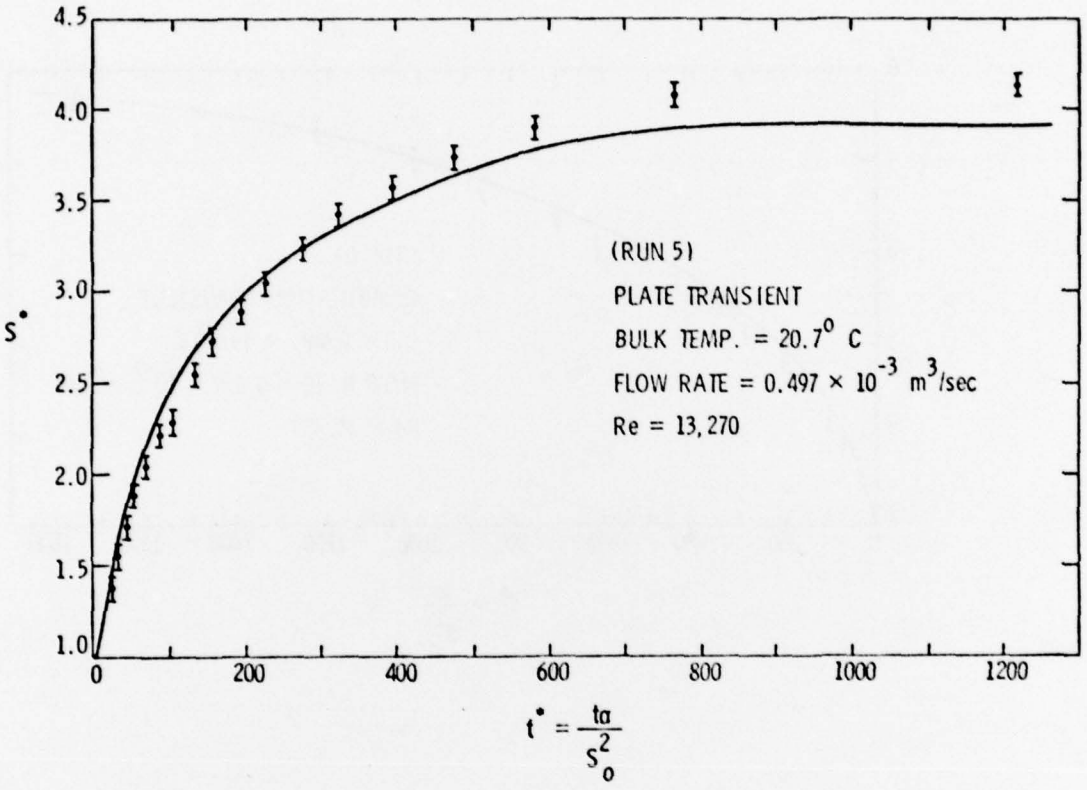

Figure 41. Results of Transient Run 5

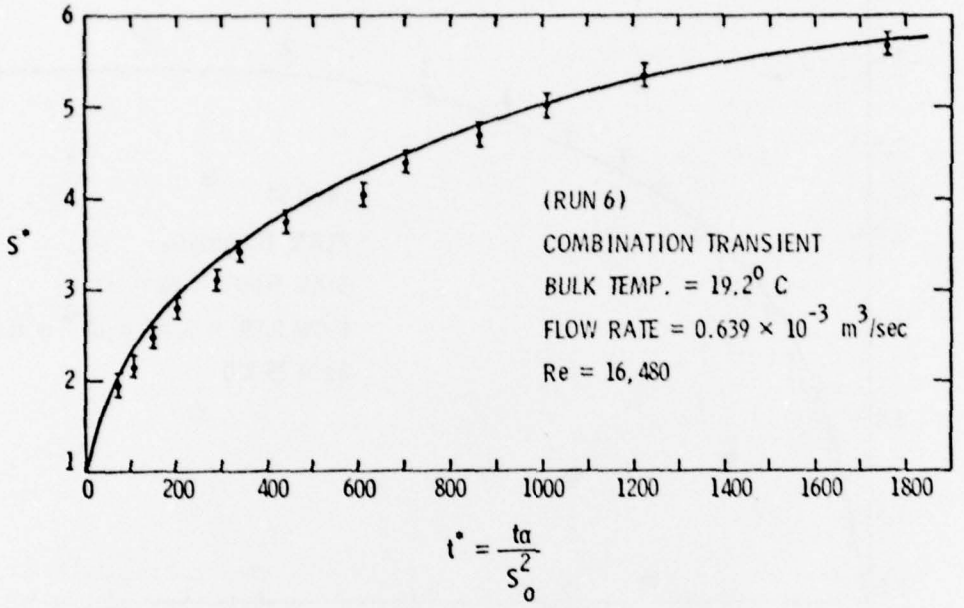

Figure 42. Results of Transient Run 6

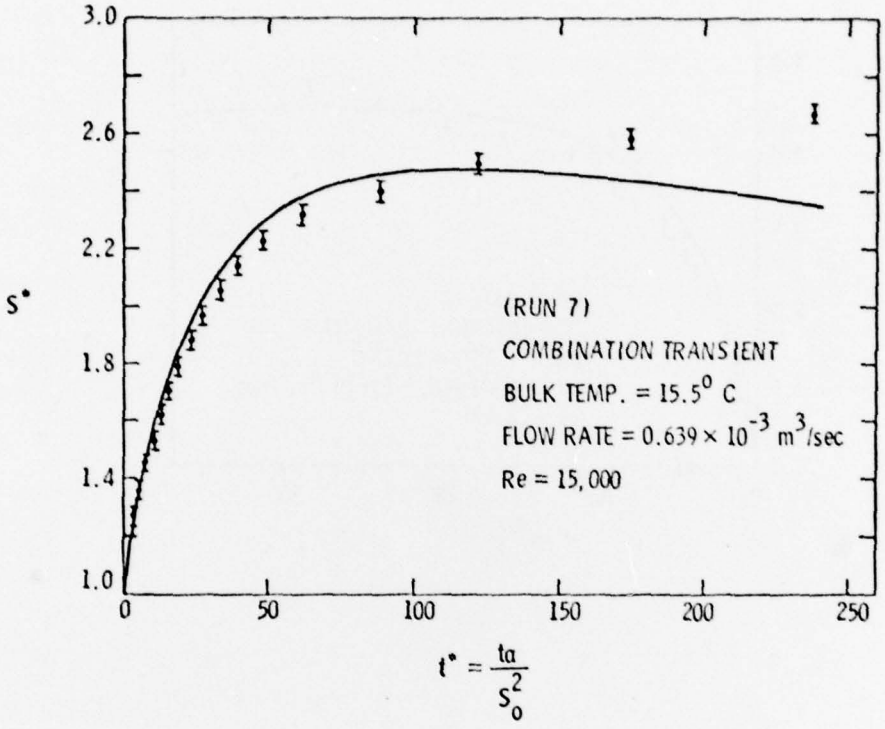

Figure 43. Results of Transient Run 7

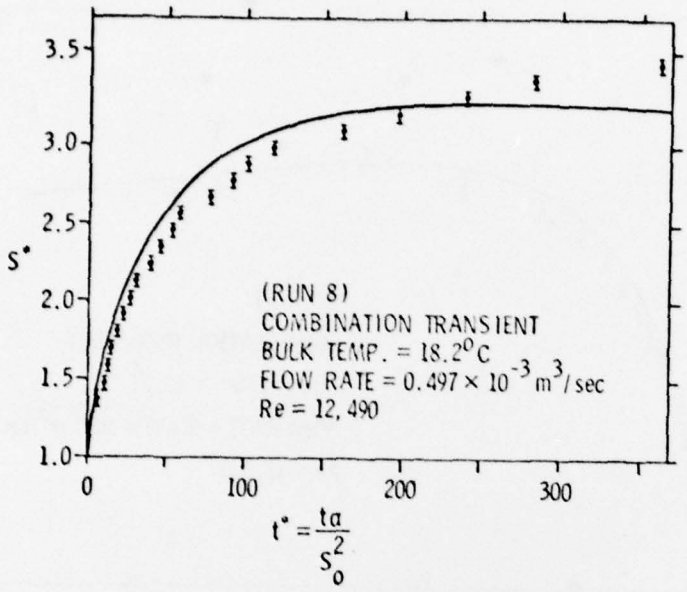

Figure 44. Results of Transient Run 8

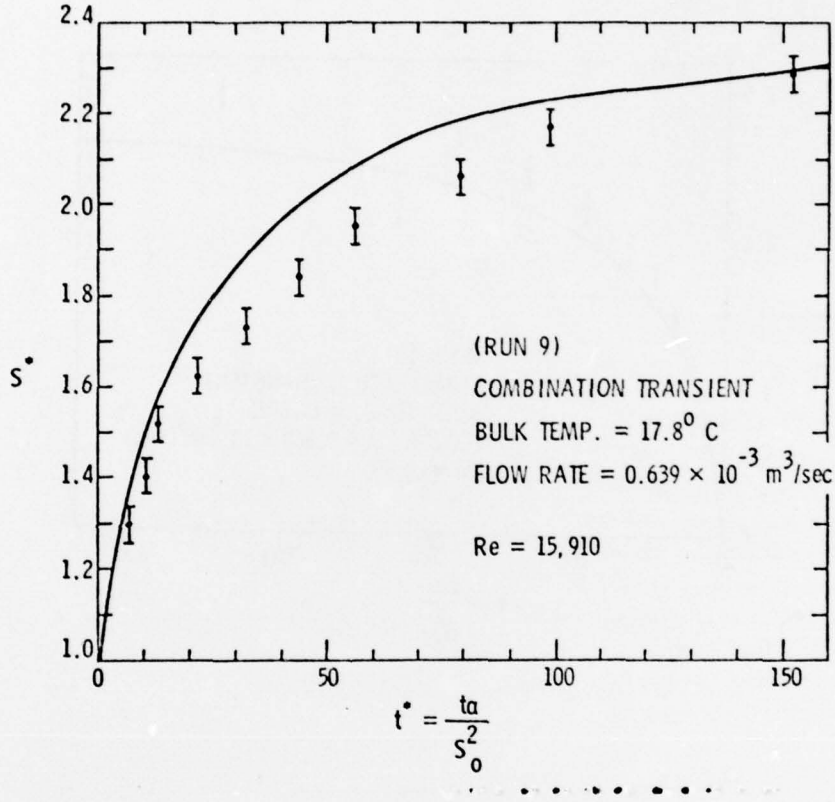

Figure 45. Results of Transient Run 9

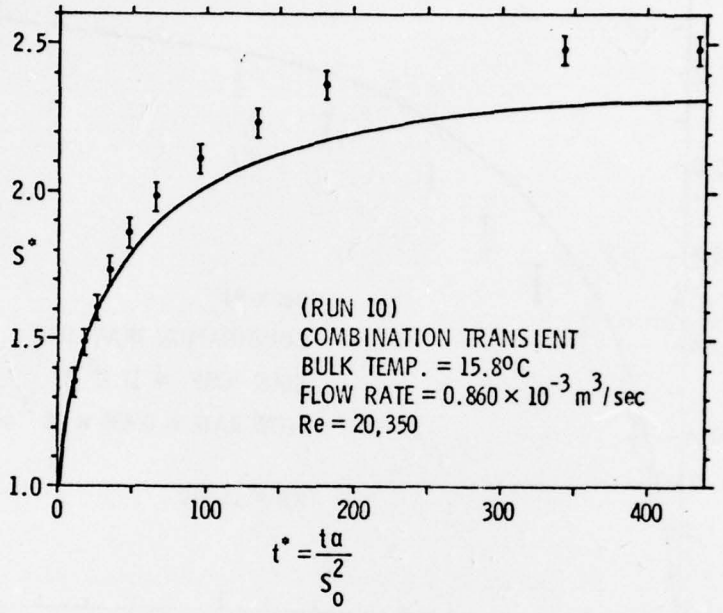

Figure 46. Results of Transient Run 10

rate at small t^* while underpredicting it at large t^*. The same is nominally true of the results for the combination plate temperature and interface heat flux transient tests (Figures 42 through 46). This effect may be due to the fact that constant transport properties were used for the ice layer in the model. In reality, the mean thermal conductivity in the layer increased by as much as 15% between the start and end of a transient run, while the conductivity of the ice near the plate surface increased by as much as 30% in a run. This variation would cause the actual layer growth to be slower than predicted at the beginning of the transient and more rapid toward the end. The value for ice thermal conductivity used throughout all transient runs was $k = 2.44 W/m-°C$ which corresponds to a mean ice layer temperature of -17.5°C (20). The conductivity (and hence, diffusivity) variation may also be partially responsible for the fact that generally better agreement was obtained in the plate transient runs because the time averaged mean temperature in the layer was substantially lower than -17.5°C in the combination transient runs. It should also be pointed out that the interface heat flux correlation used in the formation of q^* introduces an uncertainty of about $\pm 5\%$ into the estimation of this parameter. The only other factor which may have made some contribution to the deviation between experiment and theory was the analytic representation (and subsequent differentiation) of the wall or plate temperature variation during the transient runs. However, due to the overall good fit yielded by the rational function approximations and to the smooth derivatives resulting from their differentiation, it is believed that the contribution to the deviations seen in Figures 37 through 46 from this source are small.

D. Final Conclusions

The results of the transient experiments and the comparison with the model predictions essentially indicates only one major deficiency of the mathematical model; i.e., the inability to take into consideration temperature dependent solid layer properties. The other factors mentioned above which may have contributed to the discrepency between experiment and theory result from uncertainties in the model input data rather than from any of the fundamental assumptions made in the model formulation. In an attempt to estimate the seriousness of this deficiency with respect to the practical application of the model, one factor must be kept in mind; the substance used in the present experimental investigation is not necessarily a typical one with respect to the degree to which its transport properties depend on temperature near the fusion temperature. It is true that dielectric solids such as ice may exhibit a substantial variation in thermal conductivity with temperature [see Dillard (22)]. However, most substances, pure metals, for example, which commonly occur in melting and solidification phenomena have thermal conductivities and diffusivities which are not nearly as dependent on temperature as are the corresponding properties of ice [see (23) and (24)]. It is therefore expected that the failure of the model to account for varying transport properties would be found much less significant in experiments conducted with these substances. An extension of the present work might attempt to account for the variation of the solid phase properties with temperature in the finite difference model.

In the final evaluation of the mathematical model, it is noted that even if the property variation of ice is considered typical, the results in Figures 37 through 46 indicate basically good agreement between

experiment and theory, and the remaining assumptions and simplifications made in the model formulation (other than that of constant solid layer properties) seem to be justified by the experimental results. It is therefore concluded that the mathematical model and calculation procedure outlined here does provide an effective means of predicting the behavior of the simple, two-phase system shown in Figure 1 under conditions of practical engineering interest.

REFERENCES

1. Cheung, F. B. and L. Baker Jr., "Transient Freezing of Liquids in Tube Flow," Nuclear Science and Engineering, Vol. 60, p. 1-9, 1976.

2. Stefan, J., "Uber die Theorie der Eisbildung, insbesondere über die Eisbildung im Polarmeere," Annalen der Physik und Chemie, Vol. 42, p. 269, 1891.

3. Portnov, I. G., "Exact Solution of the Freezing Problem With Arbitrary Temperature Variation on the Fixed Boundary," Soviet Physics, Vol. 7, No. 3, p. 186, 1962.

4. Stephan, K., "The Influence of Heat Transfer on Melting and Solidification in Forced Flow," Int. J. Heat Mass Transfer, Vol. 12, p. 199-214, 1969.

5. Goodman, T. R., "The Heat Balance Integral and Its Application to Problems Involving a Change of Phase," Trans. A.S.M.E., Vol. 80, p. 335-342, 1958.

6. Libby, P. A. and S. Chen, "The Growth of a Deposited Layer on a Cold Surface," Int. J. Heat Mass Transfer, Vol. 8, p. 395-402, 1965.

7. Savino, J. M. and R. Siegel, "Experimental and Analytical Study of the Transient Solidification of a Warm Liquid Flowing Over a Chilled Flat Plate," NASA TN D-4015, 1967.

8. Biot, M. A., "New Methods in Heat Flow Analysis With Application to Flight Structures," J. Aeronaut. Sci., Vol. 24, p. 857-873, 1957.

9. Lapadula, C., and W. K. Mueller, "Heat Conduction With Solidification and a Convective Boundary Condition at the Freezing Front," Int. J. Heat Mass Transfer, Vol. 9, p. 702-704, 1966.

10. Bilenas, J. A., and L. Jiji, "Variational Solution of Axisymmetric Fluid Flow in Tubes With Surface Solidification," Journal of the Franklin Institute, Vol. 289, No. 4, April, 1970.

11. Springer, G. S., and D. R. Olson, "Method of Solution of Axisymmetric Solidification and Melting Problems," Contributed by the Heat Transfer Division for presentation at the Winter Annual Meeting, Nov. 25-30, 1962, of the ASME.

12. Murray, W. D. and F. Landis, "Numerical and Machine Solutions of Transient Heat Conduction Problems Involving Melting or Freezing," J. of Heat Transfer, ASME Trans. Series C, Vol. 81, p. 106-112, 1959.

13. E. Friedman, "An Iterative Procedure for Including Phase Change in Transient Conduction Programs and its Incorporation into the Finite Element Method," Submitted through, AIChE HT and EC Division for the 1977 National Heat Transfer Conference, Solidification and Melting Heat Transfer, p. 182.

14. Schlicting, Hermann, Boundary Layer Theory, McGraw-Hill, New York, 1968.

15. Lapidus, Leon and J. H. Seinfeld, Numerical Solution of Ordinary Differential Equations, Academic Press, New York, 1971.

16. Özisik, M. N., Boundary Value Problems of Heat Conduction, International Textbook Company, Scranton, PA., 1968.

17. Beckwith, T. G., and N. L. Buck, Mechanical Measurements, Addison-Wesley, Menlo Park, California, 1973.

18. Krieth, F., Principles of Heat Transfer, Intext Publishing Company, New York, 1976.

19. Kays, W. M., Convective Heat and Mass Transfer, McGraw-Hill, New York, 1976.

20. Ratcliffe, E. H., "The Thermal Conductivity of Ice-New Data on the Temperature Coefficient," Philosophical Magazine, Vol. 7, No. 79, p. 1197-1203, 1962.

21. Saff, E. B. and R. S. Varga, Padé and Rational Approximation (Theory and Applications), Academic Press, New York, 1977.

22. Dillard, D. S., and K. D. Timmerhaus, "Low Temperature Thermal Conductivity of Selected Dielectric Crystalline Solids," Thermal Conductivity Proceedings of the 8th Conference, Purdue Univ., West Lafayette, Indiana, Oct. 7-10, 1968.

23. Ho, C. V., Powell, R. W., and K. Y. Wu, "Thermal Diffusivity of the Elements," Thermal Conductivity Proceedings of the 8th Conference, Purdue Univ., West Lafayette, Indiana, Oct. 7-10, 1968.

24. Missenard, André, Conductivité Thermique Des Solides, Liquides, Gaz Et De Leurs Melanges, Editions Eyrolles, Paris, 1965.

APPENDIX A

FINITE DIFFERENCE APPROXIMATIONS

$$\frac{D\theta}{Dt^*} = \frac{\theta_n^{r+1} - \theta_n^r}{\Delta t^*} + O(\Delta t^*)$$

$$\frac{\partial^2\theta}{\partial y^{*2}} = \frac{\theta_{n-1}^r + \theta_{n+1}^r - 2\theta_n^r}{\Delta y^{*2}} + O(\Delta y^{*2})$$

$$\frac{\partial\theta}{\partial y^*} = \frac{\theta_{n+1}^r - \theta_{n-1}^r}{2\Delta y^*} + O(\Delta y^{*2})$$

$$\left.\frac{\partial\theta}{\partial y^*}\right|_{y^*=S^*} = \frac{\theta_{N-2}^r - 4\theta_{N-1}^r + 3\theta_N^r}{2\Delta y^*} + O(\Delta y^{*2})$$

$$\frac{dS^*}{dt^*} = \frac{S^{*r+1} - S^{*r}}{\Delta t^*} + O(\Delta t^*)$$

Equation (21a),

$$\frac{\theta_n^{r+1} - \theta_n^r}{\Delta t^*} = \frac{(\theta_{n-1}^r + \theta_{n+1}^r - 2\theta_n^r)}{\Delta y^{*2}} - \frac{1}{St}\frac{dSt}{dt^*}[\theta_n^r - 1] + \frac{y_n^*}{S^{*r}}\frac{dS^*}{dt^*}\frac{(\theta_{n+1}^r - \theta_{n-1}^r)}{2\Delta y^*} .$$

Equation (21f),

$$St\,\frac{(\theta_{N-2}^r - 4\theta_{N-1}^r + 3\theta_N^r)}{2\Delta y^*} - q^* = \frac{S^{*r+1} - S^{*r}}{\Delta t^*} .$$

$O(\,)$ denotes the order of the error term as given by Özisik, (16).

DISTRIBUTION

Commander (NSEA 09G32)
Naval Sea Systems Command
Department of the Navy
Washington, DC 20362 — Copies 1 and 2

Commander (NSEA 0342)
Naval Sea Systems Command
Department of the Navy
Washington, DC 20362 — Copies 3 and 4

Defense Documentation Center
5010 Duke Street
Cameron Station
Alexandria, VA 22314 — Copies 5 through 16